


ARTICLE

Reconstitution and mechanistic dissection of the human microtubule branching machinery

Yaqian Zhang^{1,2}, Xing Hong^{1,2}, Shasha Hua^{1,2}, and Kai Jiang^{1,2} 

Branching microtubule (MT) nucleation is mediated by the augmin complex and γ -tubulin ring complex (γ -TuRC). However, how these two complexes work together to promote this process remains elusive. Here, using purified components from native and recombinant sources, we demonstrate that human augmin and γ -TuRC are sufficient to reconstitute the minimal MT branching machinery, in which NEDD1 bridges between augmin holo complex and GCP3/MZT1 subcomplex of γ -TuRC. The single-molecule experiment suggests that oligomerization of augmin may activate the branching machinery. We provide direct biochemical evidence that CDK1- and PLK1-dependent phosphorylation are crucial for NEDD1 binding to augmin, for their synergistic MT-binding activities, and hence for branching MT nucleation. In addition, we unveil that NEDD1 possesses an unanticipated intrinsic affinity for MTs via its WD40 domain, which also plays a pivotal role in the branching process. In summary, our study provides a comprehensive understanding of the underlying mechanisms of branching MT nucleation in human cells.

Introduction

During mitosis, the equal segregation of chromosomes is carried out by the spindle, which is mainly made up of microtubules (MTs) and their associated proteins. Besides the centrosome and the vicinity of chromatin, spindle MTs can also nucleate from preexisting MTs, which is termed branching MT nucleation (Petry, 2016; Kapoor, 2017; Prosser and Pelletier, 2017). This process depends on MT nucleator γ -tubulin ring complex (γ -TuRC) and its recruiting factor augmin (Goshima and Kimura, 2010).

Augmin is a hetero-octameric protein complex that is present in vertebrates, insects, and plants but absent from yeasts and worms. By recruiting γ -TuRC, augmin-mediated branching MT nucleation is required for the assembly of metaphase spindle, especially kinetochore-fiber formation, the assembly of anaphase central spindle, and faithful cytokinesis (Goshima et al., 2007; Goshima et al., 2008; Zhu et al., 2008; Lawo et al., 2009; Uehara et al., 2009; Uehara and Goshima, 2010; Ho et al., 2011; Petry et al., 2011; Uehara et al., 2016). Augmin can also regulate the MT organization of nonmitotic cells, such as interphase plant cells (Liu et al., 2014b) and neurons (Sanchez-Huertas et al., 2016; Cunha-Ferreira et al., 2018). Studies in developing organisms have revealed that the knockout of augmin subunit *Haus6* in mice is lethal (Watanabe et al., 2016). *Drosophila* augmin is required for female fertility and the viability of flies

without functioning centrosomes (Meireles et al., 2009; Wainman et al., 2009).

The γ -TuRC, which is conserved from yeast to human but varies in composition across organisms, functions as a template for MT nucleation (Kollman et al., 2011; Zupa et al., 2021). In higher eukaryotes, γ -TuRC consists of the core components including γ -tubulin and GCP2-6, as well as some accessory components, such as NEDD1, MZT1, MZT2A/B, NME7, and actin (Zheng et al., 1995; Knop et al., 1997; Oegema et al., 1999; Haren et al., 2006; Luders et al., 2006; Choi et al., 2010; Hutchins et al., 2010; Teixeira-Travesa et al., 2010; Liu et al., 2014a). Recent cryo-EM structures of vertebrate γ -TuRC significantly advanced our understanding of its components' stoichiometry, position, and structures (Consolati et al., 2020; Liu et al., 2020; Wieczorek et al., 2020a; Wieczorek et al., 2020b; Zimmermann et al., 2020).

In the *Xenopus* system, besides augmin and γ -TuRC, TPX2 is also required for branching MT nucleation, which has been initially demonstrated in *Xenopus* egg extracts and then further confirmed using in vitro reconstitution with purified proteins (Petry et al., 2013; Alfaro-Aco et al., 2020). However, in the *Drosophila* system, TPX2 has been shown to be dispensable for this process both in vivo and in vitro (Verma and Maresca, 2019; Tariq et al., 2020). It remains to be determined which scenario

¹The State Key Laboratory Breeding Base of Basic Science of Stomatology and Key Laboratory of Oral Biomedicine Ministry of Education, School & Hospital of Stomatology, Wuhan University, Wuhan, China; ²Frontier Science Center for Immunology and Metabolism, Medical Research Institute, Wuhan University, Wuhan, China.

Correspondence to Kai Jiang: jiangkai@whu.edu.cn.

© 2022 Zhang et al. This article is distributed under the terms of an Attribution–Noncommercial–Share Alike–No Mirror Sites license for the first six months after the publication date (see <http://www.rupress.org/terms/>). After six months it is available under a Creative Commons License (Attribution–Noncommercial–Share Alike 4.0 International license, as described at <https://creativecommons.org/licenses/by-nc-sa/4.0/>).

applies to the human system. More importantly, direct observation of the behaviors of the branching factors has not been achieved by previous *in vitro* reconstitutions.

As an accessory subunit of γ -TuRC, NEDD1 is established to be the bridging factor between γ -TuRC and augmin. However, there have been inconsistencies regarding the site of the NEDD1–augmin interaction in the results reported by different groups (Zhu et al., 2008; Uehara et al., 2009; Chen et al., 2017). Moreover, the contribution of NEDD1 to branching MT nucleation has not been assessed in previous *in vitro* works. While several studies have reported that phosphorylation of NEDD1 by CDK1 is required for its binding to augmin, this has not been directly demonstrated using purified components (Luders et al., 2006; Uehara et al., 2009). Furthermore, the importance of CDK1-dependent phosphorylation in branching MT nucleation has not been highlighted in previous *in vitro* work. It also remains unclear whether other mitotic kinases are directly involved in regulating this process.

In this study, we reconstitute the minimal MT branching machinery using native and recombinant sources of the human augmin– γ -TuRC complex. Our reconstitution system allows real-time observation of both augmin and γ -TuRC behavior during branching nucleation and quantitative definition of the branching events. We unveil that NEDD1 functions as a bridging factor by binding to the augmin holo complex and γ -TuRC subcomplex formed by MZT1 and N-terminal extension of GCP3. Unexpectedly, NEDD1 also possesses an intrinsic affinity for MTs via its WD40 domain, which plays a critical role in branching nucleation. Using purified recombinant components, we provide direct evidence that CDK1- and PLK1-dependent phosphorylation are essential for NEDD1 binding to augmin, for their synergistic MT-binding activities, and hence for branching MT nucleation. Collectively, our work opens the way to detailed mechanistic studies to understand the underlying mechanisms of branching MT nucleation in the human system.

Results

Reconstitution of branching MT nucleation using purified native augmin– γ -TuRC complex

To determine whether a source of the augmin– γ -TuRC complex could be generated from human cells, we constructed a CRISPR/Cas9 HeLa knock-in cell line in which the endogenous HAUS8 protein was C-terminally fused to a GFP tag for imaging and a Strep-tag for affinity purification (Fig. S1 A). Although this cell line was heterozygous for the tag insertion based on genotyping and Western blot analyses (Fig. S1, B and C), no interaction between Strep–GFP–tagged and untagged HAUS8 was observed in the pull-down assay (Fig. S1 D), which is consistent with previous results showing that the augmin complex is a monomer in solution (Goshima et al., 2008; Lawo et al., 2009; Hsia et al., 2014; Song et al., 2018). HAUS8–GFP–Strep localized to the spindle from late prometaphase to metaphase, and the central spindle and midbody from anaphase to telophase (Fig. S1 E), as described previously, suggesting that this fusion protein is functional (Goshima et al., 2008; Zhu et al., 2008; Lawo et al., 2009). The HAUS8–GFP–Strep-containing complex was then

purified from asynchronous (interphasic) or mitotically arrested knock-in cells. Western blot analysis showed that γ -TuRC components were present in the mitotic but not interphasic Strep prep of HAUS8 (Fig. 1 A), demonstrating that γ -TuRC could copurify with augmin in a cell cycle-dependent manner, which is consistent with previous immunoprecipitation results with anti-HAUS6 antibody (Zhu et al., 2008). Of note, mitotic HAUS6, HAUS8, and NEDD1 displayed apparent band shifts, most likely caused by phosphorylation (Fig. 1 A; Zhu et al., 2008; Johmura et al., 2011). Further mass spectrometry analysis of the mitotic Strep prep of HAUS8 identified all known augmin and γ -TuRC components, except for MZT1 owing to its small size, but no additional MT-related protein factors (Fig. S1 F and Table S1, A and B).

To test whether the purified native augmin– γ -TuRC complex is sufficient to stimulate branching MT nucleation, we performed *in vitro* MT dynamics assays. GMPCPP-stabilized MTs were first attached to the surface of a flow chamber to function as seeds to initiate nucleation. Strikingly, upon addition of tubulin reaction mixture containing the augmin– γ -TuRC complex (10 nM augmin; 0.35 nM γ -TuRC), robust branching events were observed (Fig. 1 B and Video 1). Closer observation of individual seeds during the 25-min imaging window revealed that the primary, secondary, and tertiary branching events, which generated daughter, granddaughter, and great-granddaughter MTs, respectively, occurred in an ordered series and ultimately resulted in the formation of the fan-like structure (Fig. 1, C–F; and Video 2). The branched daughter MTs can originate either from GMPCPP seeds or from GDP-MTs grown from both ends of seeds (Figs. 1 C and S1 G). *De novo* nucleation of branched MTs from solution was also observed (3.5 ± 2.3 events per 88×88 - μm imaging field; arrowhead in Figs. 1 B and S1 H). Since no additional MT-associated proteins were present in this complex, these data suggest that γ -TuRC and augmin represent the minimal MT branching machinery in the human cell system, which is similar to *Drosophila* but contrasts with the *Xenopus* system, in which TPX2 is required (Alfaro-Aco et al., 2020; Tariq et al., 2020).

Branched MTs were preferentially formed in angles $<90^\circ$ and the same orientation as the mother MTs, with 10 – 30° being the most frequently observed (Fig. 1 G). Although occasionally branch angles could be $>90^\circ$, the percentage was quite low (1.7%; Figs. 1 G and S1 I).

The fractional distance distribution revealed that the branching events, irrespective of whether they were primary, secondary, or tertiary, preferentially occurred from older regions of GDP-MTs (Fig. 1, E and H; see Materials and methods for details). A similar older-region preference was observed for branching events in *Xenopus* egg extract and *Drosophila* S2 cells (Thawani et al., 2019; Verma and Maresca, 2019). However, it must be noted that in our assays branching events occurred infrequently within a short region close to the seed or the minus ends of mother MTs (0 – 10% fractional distance). This is consistent with the work in *Drosophila* S2 cells but contrasts with the results from *Xenopus* egg extract showing that the probability of branching peaked in sites closest to the minus end of mother MTs. In summary, the branching MT nucleation could be

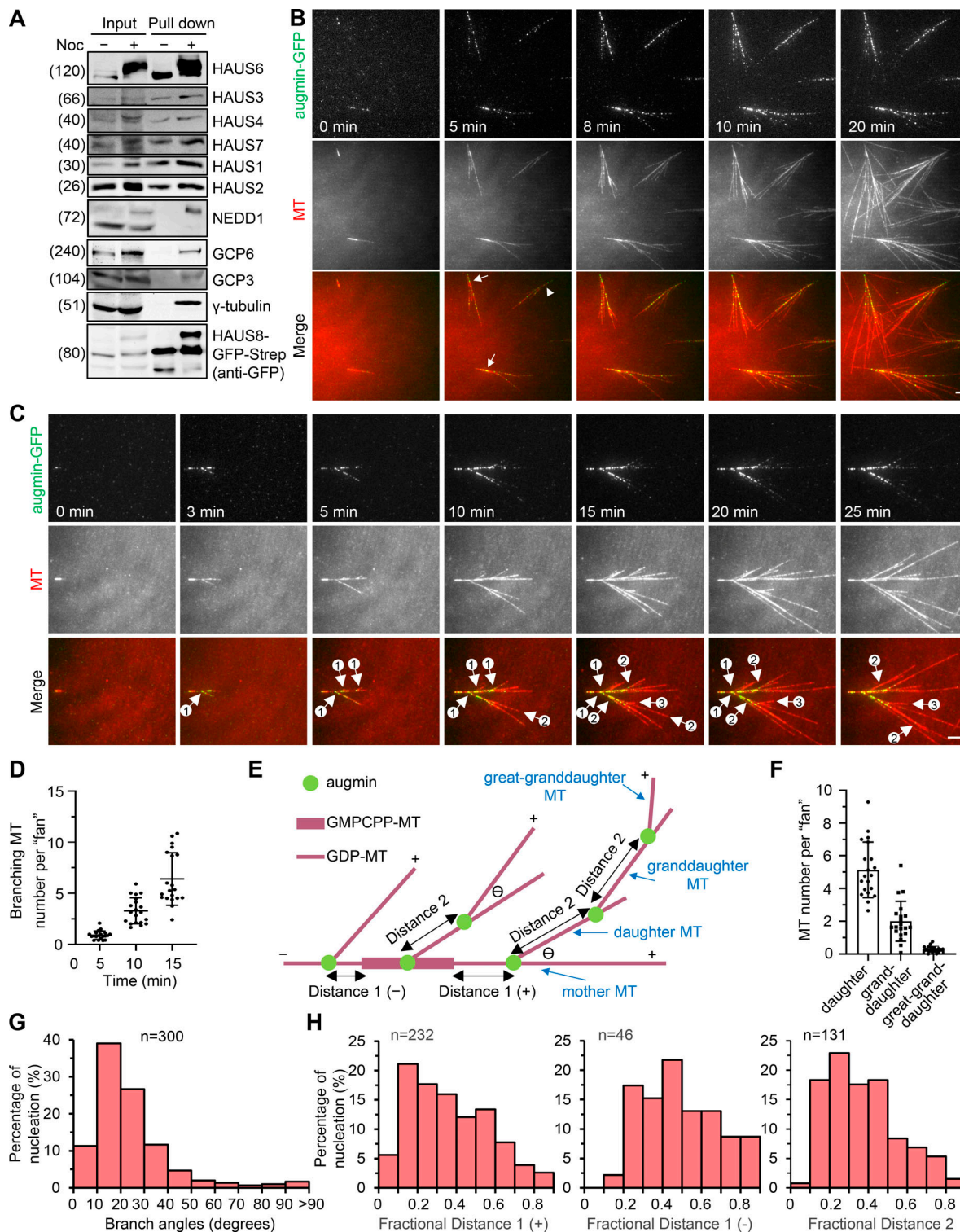


Figure 1. Reconstitution of branching MT nucleation using purified native augmin- γ -TuRC complex. (A) StrepTactin pull-down assay with extracts of HAUS8-GFP-Strep knock-in HeLa cells without or with nocodazole treatment, analyzed by Western blotting with indicated antibodies. (B) TIRF microscopy images of branching MT nucleation both from GMPCPP seeds (denoted by arrows) and from solution (denoted by arrowhead) in the presence of native augmin- γ -TuRC complex (green; 10 nM augmin; 0.35 nM γ -TuRC) purified from the nocodazole-arrested mitotic HAUS8-GFP-Strep knock-in HeLa cells. (C) TIRF microscopy images of individual branching events occurred from a single GMPCPP seed. Circled numbers indicate primary, secondary, and tertiary branches. (D) Quantification of the total number of branched MTs per fan-like structure at indicated time points for the experiments shown in B. $n = 20$ experiments. (E) Schematic representation of an ordered series of branching events that occurred from a single GMPCPP seed. θ denotes the branch angle. (F) Quantification of the number of daughter, granddaughter, and great-granddaughter MTs per fan-like structure at the 25-min time point for the experiments shown in B. $n = 20$ experiments. (G) Distribution of branch angles. $n = 300$ branch angles from 10 experiments. (H) Distribution of fractional distance. Three types of fractional distance were obtained by dividing the corresponding distance as illustrated in E by the total length of the mother MT at the time of branching. From left to right, $n = 232$, 46, and 131 from 10 experiments. Scale bars, 2 μ m. Data represent mean \pm SD.

reconstituted *in vitro* using purified native augmin- γ -TuRC complex from human cells.

Direct observation of augmin and γ -TuRC during the process of branching nucleation

To visualize the behaviors of both augmin and γ -TuRC during the process of branching nucleation, we further inserted a SNAP-tag after the last codon of GCP2 in our aforementioned cell line HAUS8-GFP-Strep (Fig. S2 A). The insertion of SNAP-tag into GCP2 was homozygous, and both tagged HAUS8 and GCP2 showed proper localization (Fig. S2, B–D). SNAP-tagged γ -TuRC were copurified with Strep-GFP-tagged augmin from this doubly genome-edited cell line and subsequently fluorescently labeled with an Alexa Fluor 647 (AF647) SNAP dye substrate (Fig. S2 E). The doubly tagged augmin- γ -TuRC complex (7.5 nM augmin; 0.15 nM γ -TuRC) could also initiate the expected branching in the *in vitro* MT dynamics assay (Fig. 2, A and C; and Videos 3 and 4). When examining the localization of augmin-GFP and γ -TuRC-SNAP/AF647, we found that ~64% γ -TuRC-SNAP/AF647-positive puncta were positive for augmin-GFP; however, only ~32% augmin-GFP-positive puncta were positive for γ -TuRC-SNAP/AF647. The fact that not 100% of γ -TuRC-SNAP/AF647-positive puncta were positive for augmin-GFP suggests that γ -TuRC-SNAP can dissociate from the complete complex after copurification. Further investigation of augmin-GFP and γ -TuRC-SNAP/AF647 double-positive puncta revealed that ~29% of them could initiate branching nucleation events (Fig. 2, A and B).

Based on the motion trajectory of augmin and γ -TuRC before branching nucleation, the branching events were categorized into two classes, which were further divided into four subclasses. In class 1, upon simultaneous binding of augmin and γ -TuRC, the augmin⁺ γ -TuRC⁺ puncta either remained static (class 1a; Fig. 2, D and F) or rapidly diffused along MTs before settling down at a defined site (class 1b; Fig. 2, D and G), followed by nucleation of branched MTs; in class 2, augmin was first deposited and either remained static or diffused along MTs. Once capturing γ -TuRC, the augmin⁺ γ -TuRC⁺ puncta either remained static (class 2a) or diffused (class 2b), followed by nucleation of branched MTs (Fig. 2, D and H). Classes 1a, 1b, and 2 (2a + 2b) account for 26.4, 65.4, and 8.2% of total events, respectively (Fig. 2 E). As the small number of class 2 events precludes meaningful analysis, only class 1 events were considered for further quantification. Fractional distance distribution revealed that the branching sites were spatially organized in a similar manner for class 1a and class 1b events (Fig. S2 F). The average lag time between the landing of augmin- γ -TuRC to the mother MT and nucleation of the daughter MT was 4.0 ± 3.4 and 5.8 ± 3.4 min for class 1a and 1b events, respectively (Fig. S2, G and H). Strikingly, under conditions of negligible photobleaching, while the γ -TuRC intensity remained largely unchanged during this lag time in different classes of branching events, a gradual accumulation of augmin was typically observed, as the augmin intensity was roughly twofold enhanced, on average (Fig. S2, I–L). Therefore, we speculate that augmin oligomerization may play an important role in activating γ -TuRC for the branching nucleation.

Using the doubly tagged augmin- γ -TuRC complex purified from knock-in cell lines, we next performed a single-molecule fluorescence intensity analysis to determine the number of augmin and γ -TuRC molecules at the branching sites. The oligomeric state of augmin and γ -TuRC in solution was first assessed by comparing the intensity of individual molecules of augmin-GFP and γ -TuRC-SNAP immobilized on the glass to the intensity of single molecules of purified GFP (monomers) or EB3-GFP (dimers), and SNAP (monomers) or EB3-SNAP (dimers), respectively. We found that augmin-GFP is monomeric in solution (Fig. 2 I); however, for γ -TuRC-SNAP, the expected peak for an intact γ -TuRC with five copies of GCP2-SNAP was not observed (Fig. 2 J), demonstrating that γ -TuRC-SNAP that copurified with Strep-GFP tagged augmin is heterogeneous in composition, containing both intact and disassembled populations. Using single molecules of GFP or SNAP immobilized in a separate chamber on the same coverslip prepared for the MT dynamics assay, we then estimated the number of augmin and γ -TuRC molecules necessary for branching nucleation. The quantitative comparison showed that, on average, the intensity of γ -TuRC-SNAP was approximately four times that of SNAP at both time points of the complex landing and branching nucleation (Fig. 2 L). Given that SNAP-tag labeling efficiency was estimated to be ~90% (see Materials and methods for details) and that one γ -TuRC molecule contains five SNAP-tagged GCP2 subunits, it is most likely that one γ -TuRC molecule is involved in the whole process of branching nucleation. In contrast, although only one augmin-GFP molecule was observed at the time point of landing, two to three augmin-GFP molecules were seen at the time point of branching nucleation (Fig. 2 K). Therefore, we conclude that in our *in vitro* system, branching MT nucleation typically occurs in two steps. The first step is the landing of one augmin molecule complexed with one γ -TuRC molecule on the MT lattice. The second step is incorporating another one or two augmin molecules into the complex, probably resulting in the activation of the branching machinery.

Reconstitution of branching MT nucleation using overexpressed recombinant augmin- γ -TuRC complex

As it is not convenient to engineer and mutate specific subunits of the native complex, for further mechanistic understanding, we attempted to get a source of overexpressed recombinant complexes. By modifying the original pTT5 vector (Durocher et al., 2002; Hua and Jiang, 2020), we set up a multigene expression system in HEK293T cells. Briefly, genes of interest were first individually cloned into our custom-designed vector pTT5Multi and then assembled into one plasmid harboring multiple gene cassettes (Fig. S3, A and B; see Materials and methods for details). We constructed two plasmids (H6/H2/H8/H3 and H7/H5/H4/H1; H is short for HAUS) for the augmin complex and three plasmids (GCP3/GCP2/ γ -tubulin/ γ -tubulin, GCP4/GCP6/GCP5, and MZT2A/MZT2B/MZT1/NME7/NEDD1) for the γ -TuRC (Fig. S3 C). A Strep-tag together with GFP or other fluorescent tags were inserted at the C-terminus of HAUS6 or GCP3 for purification and imaging (Fig. S3 C). The intact augmin or γ -TuRC were then separately isolated from HEK293T cells through a coexpression and copurification

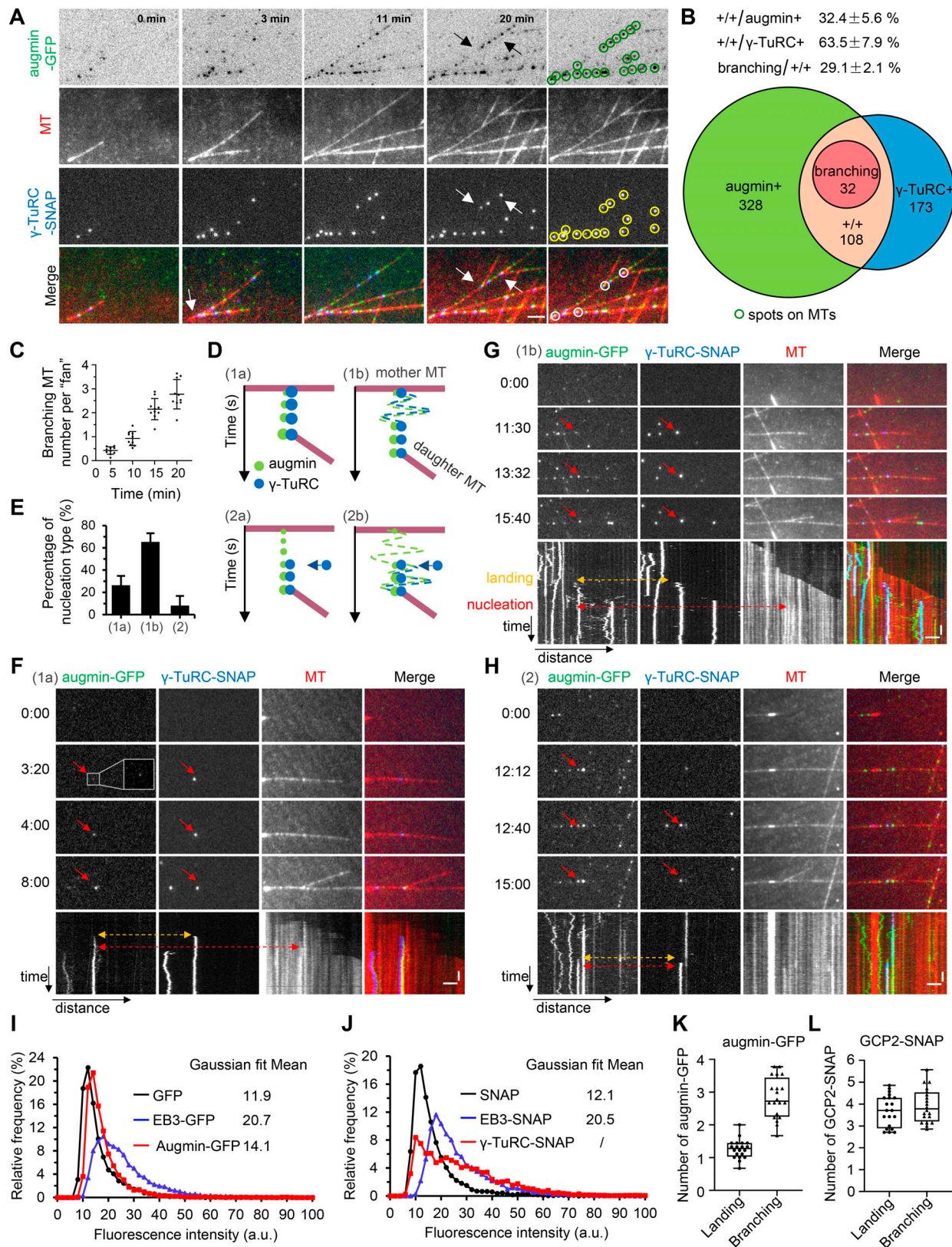


Figure 2. **Direct observation of augmin and γ -TuRC during the process of branching nucleation.** (A) TIRF microscopy images of branching MT nucleation in the presence of native augmin- γ -TuRC complex (7.5 nM augmin; 0.15 nM γ -TuRC) purified from the nocodazole-arrested mitotic HAUS8-GFP-Strep/GCP2-SNAP double knock-in HeLa cells. Arrows denote the branching sites. Green and yellow circles indicate all visible augmin-GFP-positive puncta (green) and γ -TuRC-SNAP/AF647-positive puncta (yellow) along the MTs. White circles indicate the augmin-GFP and γ -TuRC-SNAP/AF647 double-positive puncta that initiate the branching nucleation. (B) Quantification of augmin-GFP-positive puncta (augmin⁺), γ -TuRC-SNAP/AF647-positive puncta (γ -TuRC⁺), double-

positive puncta (+/+) and branching events for the experiments shown in A. Numbers in the circles were averaged from six experiments. The indicated ratios above circles represent mean \pm SD. **(C)** Quantification of the total number of branched MTs per fan-like structure at indicated time points for the experiments shown in A. $n = 10$ experiments. **(D)** Schematic representation of indicated classes of branching events. Dashed lines in the roundtrip pattern represent the diffusion step of augmin⁺ γ -TuRC⁺ puncta (1b) and augmin⁺ puncta (2b). Blue arrows indicate the time point when γ -TuRC was captured by augmin (2a and 2b). **(E)** Quantification of indicated classes of branching events. 2: 2a + 2b. $n = 8$ experiments. **(F–H)** TIRF microscopy images and kymographs showing class 1a (F), class 1b (G), and class 2 (H) branching events. The red arrows indicate the puncta that eventually initiate branching nucleation. The yellow dashed line with two-direction arrowheads indicates the time point of augmin and γ -TuRC landing (in F and G) or augmin landing (in H). The red dashed line with two-direction arrowheads indicates the time point of branching nucleation. The inset shows an enlargement of the boxed area. **(I and J)** Distribution of fluorescence intensities for single molecules of purified GFP, EB3-GFP, and augmin-GFP (I) as well as SNAP, EB3-SNAP, and γ -TuRC-SNAP (J). The means of Gaussian distribution fitting are indicated. For all conditions, $n = 5,000$ molecules from three experiments. **(K and L)** The plot of the number of augmin-GFP (K) or GCP2-SNAP (L) molecules at the time point of landing and branching nucleation. The values were obtained by dividing the intensity of augmin-GFP (K) or γ -TuRC-SNAP (L) at branch sites by the fitted mean intensity of GFP (K) or SNAP (L), respectively, in parallel chambers. $n = 20$ branching events. Horizontal scale bar, 2 μ m; vertical scale bar, 1 min. Data represent mean \pm SD.

strategy. Individual components of augmin or γ -TuRC could be readily visualized on SDS-PAGE by Coomassie blue staining, except for MZT1, MZT2A, and MZT2B owing to their low molecular weight (Fig. S3, D and E). Mass spectrometry analysis of the resulting complexes confirmed the presence of all 8 overexpressed augmin subunits or 11 overexpressed γ -TuRC subunits listed above (Table S1, C–F). Of note, although the plasmids we designed did not carry the gene cassette of actin, a factor in the “luminal bridge” of γ -TuRC (Consolati et al., 2020; Liu et al., 2020; Wiczorek et al., 2020; Zimmermann et al., 2020), endogenous actin could be copurified with other overexpressed subunits as revealed by mass spectrometry (Table S1, E and F). We should also mention that because high ionic strength was used to prepare augmin, no peptides from any γ -TuRC subunits were detected in augmin preparations. In contrast, γ -TuRC could be prepared only under low-ionic-strength buffer conditions to maintain its integrity, and a few peptides of augmin subunits were detected in γ -TuRC preparations. However, as demonstrated below, such a small amount of copurified augmin had little impact on the behavior of γ -TuRC.

To determine whether the purified complexes were active, we performed *in vitro* MT dynamics assays. As previously reported, augmin displayed MT binding affinity (Hsia et al., 2014; Song et al., 2018), and a dose-dependent increase in MT binding was observed; at 4 and 10 nM, augmin exhibited a punctate distribution pattern along MTs, and in most cases, the augmin puncta could diffuse at 4 nM but remain static at 10 nM; at 20 nM, a strong lattice decoration was observed (Fig. 3, A and E). Interestingly, augmin showed time-dependent accumulation and hence the biased distribution toward older regions of GDP lattices, with the tendency being more prominent at 10 and 20 nM; especially at 10 nM, the progressive increase in the intensity of augmin puncta was most evident (Fig. 3, A–D). The purified γ -TuRC also displayed the expected nucleation activity *in vitro*. Increasing concentrations of γ -TuRC produced increasing numbers of MTs (Fig. S3, F–H). Moreover, we found that only γ -TuRC in solution could nucleate MTs, whereas the MT lattice-bound pool of γ -TuRC failed to do so, suggesting that binding to lattice may lock γ -TuRC in a nucleation-incompetent conformation (Video 5). On closer inspection, a single MT grown from a green dot of γ -TuRC could be readily observed (Fig. 3 F). These data indicate that our purified recombinant complexes are functional.

Next, we examined the combined activity of augmin and γ -TuRC *in vitro*. Our initial attempts were to add the separately

purified augmin and γ -TuRC together. Although the accumulation of augmin and γ -TuRC along MTs was both three- to fourfold enhanced in the presence of each other, no branching was observed (Fig. 3 G; and Fig. S3, I and J). We then used an alternative strategy to isolate the complete augmin- γ -TuRC complex by simultaneous coexpression and copurification of all the components, with HAUS6 being the only component inserted with the Strep-tag for purification (Fig. S3 K; see Materials and methods for details). Mass spectrometry confirmed the presence of all components of augmin and γ -TuRC in the resulting complete complex (Table S1, G and H). *In vitro* MT dynamics assay revealed that this complete complex (10 nM augmin; 0.62 nM γ -TuRC) could potentially initiate MT branching nucleation (Fig. 3 H; Fig. S3, L and M; and Videos 6 and 7). The distribution of branch angles was similar to that observed with the purified native complex (Fig. S3 N). To find explanations for the discrepancy between these two strategies, we performed Western blot analysis. In contrast to the separately purified γ -TuRC, NEDD1 in the copurified complete augmin- γ -TuRC complex was strongly upshifted (denoted by an asterisk; Fig. 3 I), demonstrating that the copurification strategy can enrich the fraction of phosphorylated NEDD1 and suggesting that NEDD1 phosphorylation is essential for branching nucleation. Collectively, we can reconstitute branching MT nucleation using recombinant complete augmin- γ -TuRC complex from human cells through a copurification strategy.

CDK1- and PLK1-dependent phosphorylation is crucial for augmin- γ -TuRC interaction and hence for branching MT nucleation

Previous studies showed that substitution of NEDD1 S411, generally regarded as the CDK1 phosphorylation site, by alanine (S411A) can impair the spindle localization of γ -TuRC and NEDD1's binding to augmin (Luders et al., 2006; Uehara et al., 2009), and that PLK1 activity is required for the spindle localization of augmin and γ -TuRC (Haren et al., 2009; Zhu et al., 2009). We wondered whether we could provide direct biochemical evidence of the roles of these two kinases in the link between augmin and γ -TuRC. We first tested the effect of phosphorylation by CDK1 or PLK1 on the native augmin- γ -TuRC complex formation. As in Fig. 1 A, components of γ -TuRC could copurify with augmin from the mitotically arrested HAU8-GFP-Strep knock-in cell line; however, upon addition of CDK1 inhibitor RO3306 or PLK1 inhibitor BI2536 in a time-course

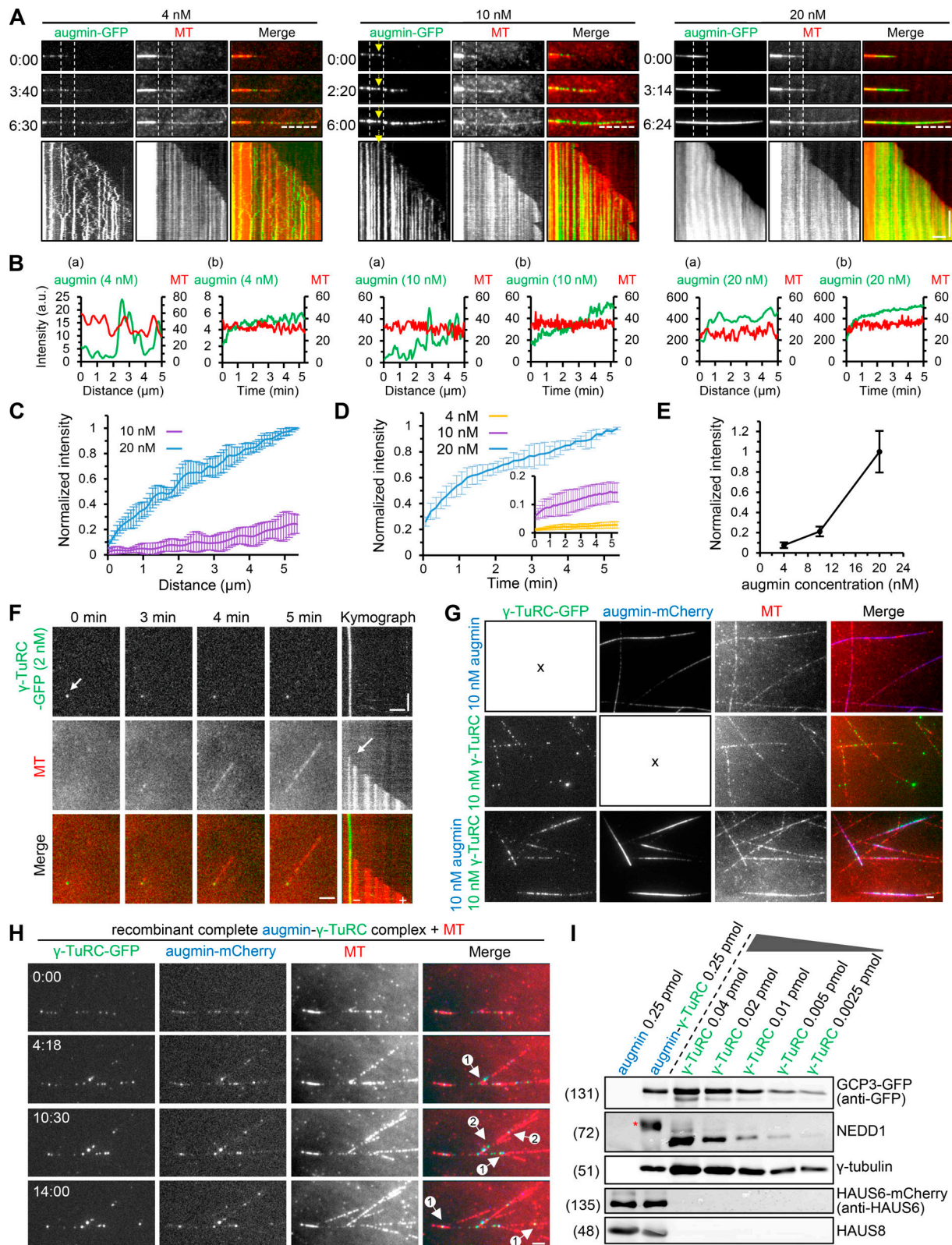


Figure 3. Reconstitution of branching MT nucleation using overexpressed recombinant augmin- γ -TuRC complex. (A) TIRF microscopy images and kymographs of MTs (red) grown in the presence of recombinant augmin-GFP (green) at indicated concentrations. Yellow arrows track one augmin-GFP punctum, the intensity of which progressively increases over time. **(B–D) (Ba)** Fluorescence intensity profiles along the MT (denoted by the horizontal dashed line in A) for indicated concentrations of augmin-GFP (green) and tubulin channel (red), showing stronger augmin-GFP intensity on older GDP-MT lattice. The origin of the x-axis represents the plus end of MT. Intensity profiles obtained from 20 different MTs were averaged and plotted in C, and the values were normalized to the maximum intensity of 20 nM augmin. **(Bb)** Mean intensity of indicated concentrations of augmin-GFP (green) and tubulin channel (red) along

a 2- μ m-long segment of GDP-MT (between two vertical dashed lines in A) over time, showing time-dependent accumulation of augmin-GFP. The mean intensity of indicated concentrations of augmin-GFP over time from 20 different MTs was averaged and plotted in D, and the values were normalized to the maximum intensity of 20 nM augmin. (E) Quantification of intensities of indicated concentrations of augmin-GFP along GDP lattice after 10 min of GDP-MT growth from seed. The values were normalized to the intensity of 20 nM augmin. $n = 60$ MTs from three experiments. (F) TIRF microscopy images and kymographs showing nucleation of an MT (red) from a single γ -TuRC-GFP (green) dot (arrows). (G) TIRF microscopy images of MTs (red) grown in the presence of 10 nM augmin-mCherry (blue; upper panels), 10 nM γ -TuRC-GFP (green; middle panels), or their combination (lower panels). Recombinant augmin-mCherry and γ -TuRC-GFP were separately purified from HEK293T cells. (H) TIRF microscopy images of branching MT nucleation in the presence of recombinant complete augmin- γ -TuRC complex (10 nM augmin; 0.62 nM γ -TuRC) copurified from nocodazole-arrested mitotic HEK293T cells expressing augmin-mCherry-Strep and γ -TuRC-GFP. Circled numbers indicate primary and secondary branches. (I) Western blot analysis of the separately purified recombinant augmin-mCherry and γ -TuRC-GFP as well as the copurified complete augmin-mCherry- γ -TuRC-GFP complex with indicated antibodies. The red asterisk indicates the up-shifted band of NEDD1. Horizontal scale bar, 2 μ m; vertical scale bar, 2 min. Data represent mean \pm SD.

manner, γ -TuRC components were reduced or not detected in the Strep prep of HAUS8 (Fig. 4, A and B). Similar to that observed for the native complex, the binding between the over-expressed augmin and γ -TuRC was dramatically reduced upon inhibition of CDK1 or PLK1; moreover, combined inhibition of these two kinases had additive effects (Fig. 4 C). Conversely, an increase in this binding was visible in the presence of co-expressed CDK1/cyclin B or PLK1, and the increase was even more obvious in the presence of both kinases (Fig. 4 D). These data confirm the critical role of CDK1- and PLK1-dependent phosphorylation in the augmin- γ -TuRC interaction. We then expressed and purified the recombinant complete augmin- γ -TuRC complex in the absence or presence of CDK1/cyclin B, PLK1, or their combination, which we refer to as augmin- γ -TuRC, augmin- γ -TuRC^{CDK1}, augmin- γ -TuRC^{PLK1}, and augmin- γ -TuRC^{CDK1/PLK1}, respectively. Consistent with the results of pull-down assays, the γ -TuRC/augmin molar ratio was lowest in augmin- γ -TuRC (0.067:1), higher in augmin- γ -TuRC^{PLK1} (0.074:1) and augmin- γ -TuRC^{CDK1} (0.075:1), and highest in augmin- γ -TuRC^{CDK1/PLK1} (0.10:1; Fig. S3 O). These complexes with the same augmin concentration (10 nM) were then applied into in vitro MT dynamics assay. As expected, although augmin- γ -TuRC was sufficient to stimulate branching, augmin- γ -TuRC^{CDK1}, augmin- γ -TuRC^{PLK1}, and augmin- γ -TuRC^{CDK1/PLK1} could stimulate branching in a more robust manner, with the effect of augmin- γ -TuRC^{CDK1/PLK1} being the most evident (Fig. 4, E and F; and Video 8). Upon closer inspection, we found that the increased branching events correlated with increased augmin and γ -TuRC intensity along MTs (Fig. 4 G). We conclude that CDK1- and PLK1-dependent phosphorylation are essential for the formation of the augmin- γ -TuRC complex and hence for branching MT nucleation.

NEDD1 specifically binds to γ -TuRC subcomplex formed by MZT1 and N-terminal extension of GCP3

Having established that the augmin- γ -TuRC interaction was regulated by CDK1- and PLK1-dependent phosphorylation, we then set out to investigate the details of this regulation. As NEDD1 is established to be the bridging factor between γ -TuRC and augmin, we first tested whether phosphorylation influences NEDD1 binding to γ -TuRC. For this purpose, the expression cassette of NEDD1 was removed from the plasmids constructed for γ -TuRC as mentioned above (γ -TuRC^{ΔNEDD1}-GFP; Fig. S3 C). Streptavidin pull-down assays revealed that neither the presence of coexpressed CDK1/cyclin B or PLK1 nor their inhibitors

affected the interaction between NEDD1 and other subunits of γ -TuRC, indicating that CDK1- and PLK1-dependent phosphorylation are not essential for the incorporation of NEDD1 into γ -TuRC (Fig. 5, A and B).

Previous work has shown that MZT1 is required for NEDD1 to interact with γ -TuRC and that MZT1 directly binds to the N-terminal fragments of GCP3, GCP5, and GCP6 (Cota et al., 2017). Our pull-down assays revealed that NEDD1 was preferentially associated with the GCP3/MZT1 subcomplex, but not MZT1 alone, GCP3 alone, or subcomplexes formed by GCP4/GCP5/GCP6/MZT1 or GCP2/MZT2 (Fig. 5, C and D; and Fig. S4 A). Recent structural studies revealed that GCP3's N-terminal helix domain (termed N-terminal extension 1 [NTE1] in this study) intercalates with MZT1 (Huang et al., 2020; Wiczorek et al., 2020; Zimmermann et al., 2020). Our pull-down assay showed that MZT1/GCP3-NTE1 was not sufficient to associate with NEDD1, whereas the presence of a linker region adjacent to NTE1 (NTE2 or NTE3) can promote the formation of the tripartite module, with the effect of NTE3 being stronger than that of NTE2 (Fig. 5, E and F). Consistent with previous results showing that the C-terminal coiled-coil (CC) domain of NEDD1 binds to γ -TuRC (Haren et al., 2006; Luders et al., 2006), our pull-down assay validated that NEDD1 CC forms a complex with MZT1/GCP3-NTE3 (Fig. 5, G and H). According to recent cryo-EM structures, only one copy of MZT1/GCP3-NTE is found in the luminal bridge, where NEDD1 is not visible. Therefore, we hypothesize that NEDD1 associates with other flexible copies of MZT1/GCP3-NTE, which may be located at the outer face of γ -TuRC (Fig. 5 I).

Phosphorylation of NEDD1 but not augmin is essential for the NEDD1-augmin interaction

Although NEDD1 has been reported by different groups to bind augmin, there is controversy regarding the site of this interaction (Zhu et al., 2008; Uehara et al., 2009; Chen et al., 2017; Song et al., 2018). Therefore, we first performed a pull-down assay to address this question. Unexpectedly, in our hands, NEDD1 interacted with the augmin holo complex but not its individual subunits or subcomplexes (Fig. 6 A). Further domain mapping revealed that a C-terminal fragment C1 (residues 391–660) of NEDD1 is necessary and sufficient for binding to augmin (Fig. 6, B and C). Interestingly, S411, which is generally regarded as the CDK1 phosphorylation site and is important for NEDD1-augmin interaction, is present in this region (Luders et al., 2006; Uehara et al., 2009). Our in vitro kinase assay and pull-down assay

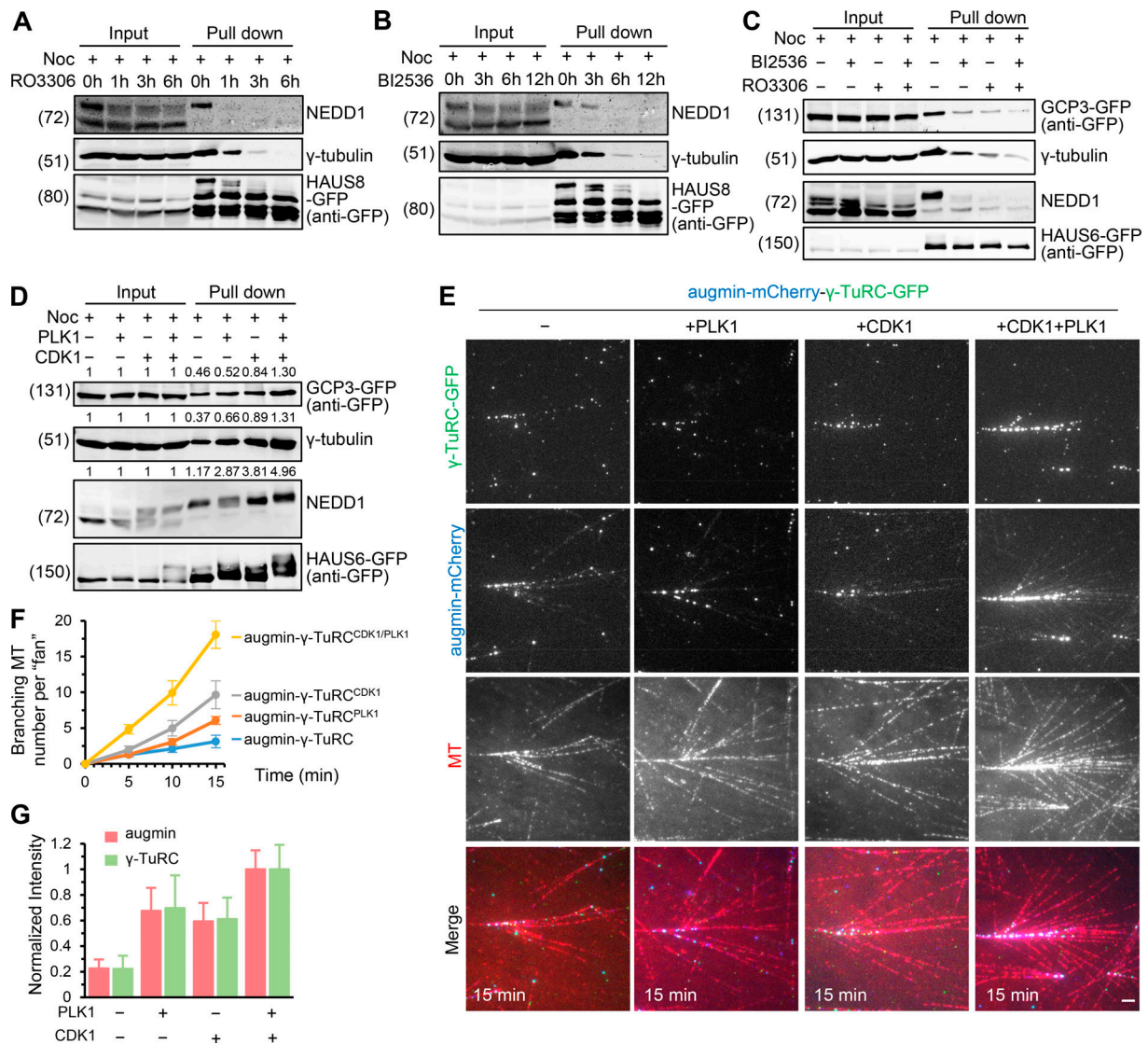


Figure 4. CDK1- and PLK1-dependent phosphorylation is crucial for augmin- γ -TuRC interaction and hence for branching MT nucleation. (A and B) StrepTactin pull-down assay with extracts of nocodazole-arrested mitotic HAUS8-GFP-Strep knock-in HeLa cells treated with CDK1 inhibitor RO3306 (A) or PLK1 inhibitor BI2536 (B) for indicated time periods, analyzed by Western blotting with indicated antibodies. **(C and D)** Streptavidin pull-down assay with extracts of nocodazole-arrested mitotic HEK293T cells expressing augmin-GFP-Bio (bait) and γ -TuRC-GFP (prey), treated with (+) or without (-) RO3306, BI2536, or both (C); or together with (+) or without (-) untagged CDK1/cyclin B, HA-PLK1, or both (D), analyzed by Western blotting with indicated antibodies. **(E)** TIRF microscopy images of branching MT nucleation in the presence of recombinant complete augmin- γ -TuRC complex (10 nM augmin) copurified from nocodazole-arrested mitotic HEK293T cells expressing augmin-mCherry-Strep and γ -TuRC-GFP, together with or without untagged CDK1/cyclin B, HA-PLK1, or both. The concentrations of γ -TuRC were 0.67, 0.74, 0.75, and 1.0 nM for augmin- γ -TuRC, augmin- γ -TuRC^{PLK1}, augmin- γ -TuRC^{CDK1}, and augmin- γ -TuRC^{CDK1/PLK1}, respectively. Images were acquired 15 min after imaging. **(F)** Quantification of the total number of branched MTs per fan-like structure at indicated time points in the assays performed with indicated complexes. $n = 3$ experiments. **(G)** Quantification of intensities of augmin-mCherry and γ -TuRC-GFP along MTs for the experiments shown in E. The values were normalized to the intensity of the augmin- γ -TuRC^{CDK1/PLK1} complex. $n = 30$ MTs from three experiments. Scale bar, 2 μ m. Data represent mean \pm SD.

further confirmed these results (Fig. S4, B and C). To address the respective contribution of NEDD1 phosphorylation and augmin phosphorylation to their connection, we produced Strep-GFP-tagged augmin holo complex and flag-tagged NEDD1 in HEK293T cells in the presence of coexpressed CDK1/cyclin B, PLK1, or their inhibitors, which we refer to as augmin^{CDK1}, augmin^{PLK1}, augmin^{RO}, augmin^{BI}, NEDD1^{CDK1}, NEDD1^{PLK1}, NEDD1^{RO}, or NEDD1^{BI}, respectively. After affinity purification, all versions of augmin were immobilized on StrepTactin beads, and all

versions of NEDD1 were eluted from the flag beads (Fig. 6, D and E). Subsequent pull-down assays using these purified proteins showed that NEDD1^{CDK1} or NEDD1^{PLK1} could be pulled down by all versions of augmin; however, NEDD1^{RO} or NEDD1^{BI} failed to be pulled down by any of them (Fig. 6, F and G). These data demonstrate that phosphorylation of NEDD1 by CDK1 and PLK1 is the key determinant of the NEDD1-augmin interaction, whereas phosphorylation of augmin is dispensable for this interaction.

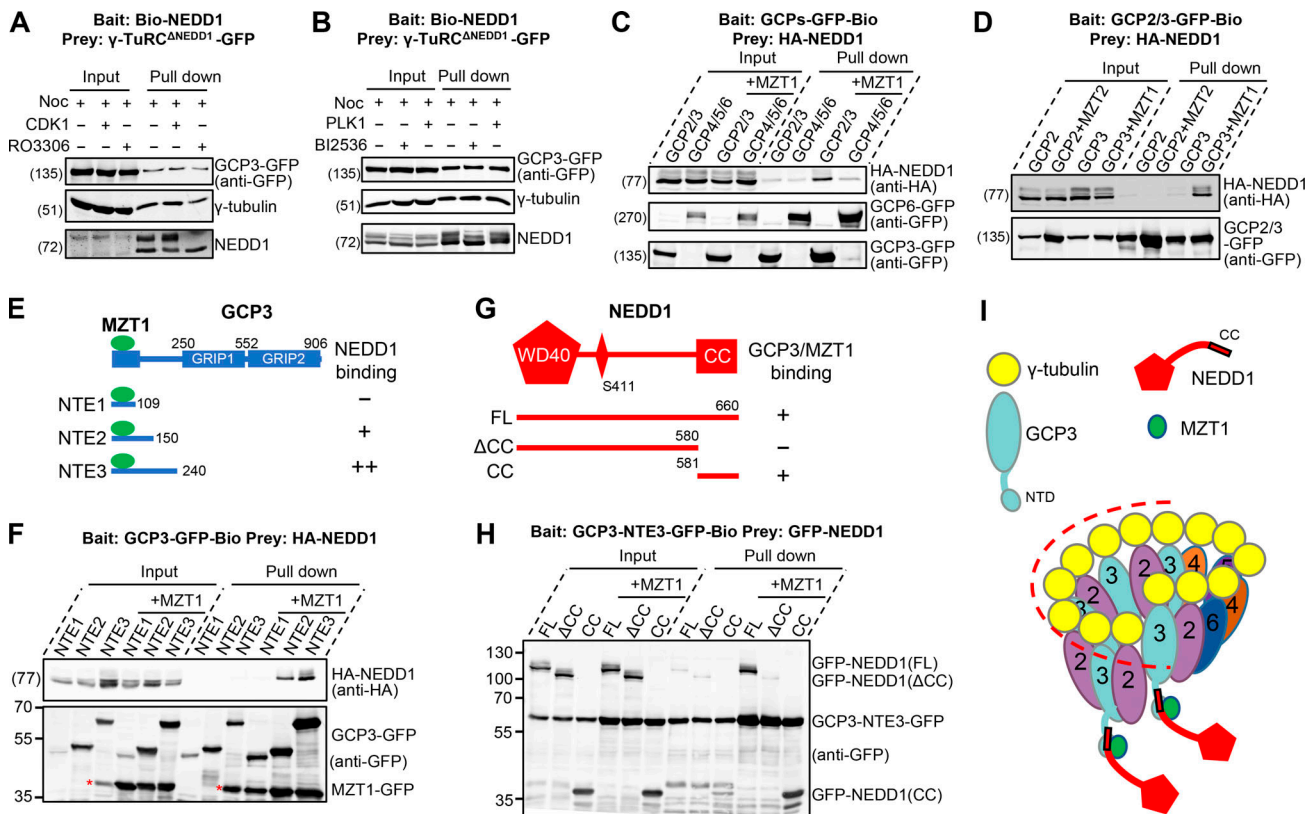


Figure 5. NEDD1 specifically binds to MZT1/GCP3 NTE subcomplex of γ -TuRC. (A and B) Streptavidin pull-down assays with extracts of nocodazole-arrested mitotic HEK293T cells expressing Bio-NEDD1 (bait) and γ -TuRC^{ANEDD1}-GFP (prey), together with (+) or without (-) untagged CDK1/cyclin B (A) or HA-PLK1 (B), treated with (+) or without (-) RO3306 (A) or BI2536 (B), analyzed by Western blotting with indicated antibodies. (C) Streptavidin pull-down assay with extracts of nocodazole-arrested mitotic HEK293T cells expressing HA-NEDD1 (prey) together with GCP2/GCP3-GFP-Bio/ γ -tubulin, GCP4/GCP5/GCP6-GFP-Bio/ γ -tubulin, GCP2/GCP3-GFP-Bio/ γ -tubulin/MZT1, or GCP4/GCP5/GCP6-GFP-Bio/ γ -tubulin/MZT1 (bait), analyzed by Western blotting with indicated antibodies. (D) Streptavidin pull-down assay with extracts of nocodazole-arrested mitotic HEK293T cells expressing HA-NEDD1 (prey) together with GCP2-GFP-Bio/ γ -tubulin, GCP2-GFP-Bio/ γ -tubulin/MZT2, GCP3-GFP-Bio/ γ -tubulin, or GCP3-GFP-Bio/ γ -tubulin/MZT1 (bait), analyzed by Western blotting with indicated antibodies. (E) Schematic overview of the domain organization of GCP3 and the deletion mutants, and summary of their interactions with NEDD1. The green ellipse represents MZT1. NTE, N-terminal extension. (F) Streptavidin pull-down assay with extracts of nocodazole-arrested mitotic HEK293T cells expressing HA-NEDD1 (prey) and Bio-GFP-tagged GCP3-NTEs together with or without MZT1-GFP (bait), analyzed by Western blotting with indicated antibodies. The asterisks indicate the degradation bands of GCP3-NTE3. (G) Schematic overview of the domain organization of NEDD1 and the deletion mutants, and summary of their interactions with GCP3/MZT1. WD40, WD-40 repeat domain. (H) Streptavidin pull-down assay with extracts of nocodazole-arrested mitotic HEK293T cells expressing GFP-tagged NEDD1 full length (FL) or indicated deletion mutants (prey) and GCP3-NTE3-GFP-Bio together with or without untagged MZT1 (bait), analyzed by Western blotting with GFP antibody. (I) Model of the interaction between NEDD1 and GCP3/MZT1 in the context of the γ -TuRC complex. The dashed line surrounding half of the cone-shaped γ -TuRC, where GCP3 was positioned, indicates the asymmetric arrangement of NEDD1 within γ -TuRC.

Both γ -TuRC phosphorylation and augmin phosphorylation are necessary for the branching nucleation and for their synergistic MT-binding activities

As mentioned above (Fig. 3), the combination of separately purified recombinant augmin and γ -TuRC is insufficient to stimulate branching. We then wondered whether increasing phosphorylation levels of the individual complexes could overcome this problem. To this end, augmin and γ -TuRC were separately produced in the presence of both coexpressed CDK1/cyclin B and PLK1 or both of their inhibitors. Based on the importance of NEDD1 phosphorylation in the augmin- γ -TuRC connection, to enrich for the fraction of phosphorylated NEDD1, γ -TuRC was prepared by moving the Strep-tag from the aforementioned GCP3 subunit to NEDD1 (see Materials and methods for details). These purified complexes were referred to

as augmin^{CDK1/PLK1}, augmin^{RO/BI}, γ -TuRC^{StN/CDK1/PLK1}, and γ -TuRC^{StN/RO/BI}, respectively (St is short for Strep-tag; N is short for NEDD1; Fig. S4, D and E). Mixtures of different versions of augmin and γ -TuRC were then applied to the in vitro MT dynamics assays. We found that the augmin^{CDK1/PLK1}- γ -TuRC^{StN/CDK1/PLK1} pair could induce the expected robust branching, whereas other pairs (augmin^{CDK1/PLK1}- γ -TuRC^{StN/RO/BI}, augmin^{RO/BI}- γ -TuRC^{StN/CDK1/PLK1}, and augmin^{RO/BI}- γ -TuRC^{StN/RO/BI}) were all less potent to do so (Fig. 6, H and I; Fig. S4 F; and Video 9). These data demonstrate that the insufficiency of a simple mixture strategy (see Fig. 3) could indeed be bypassed by increasing phosphorylation levels of augmin and γ -TuRC individually. Although for the augmin- γ -TuRC interaction, only phosphorylation of NEDD1 but not augmin is crucial, for the robust branching, both augmin phosphorylation and NEDD1

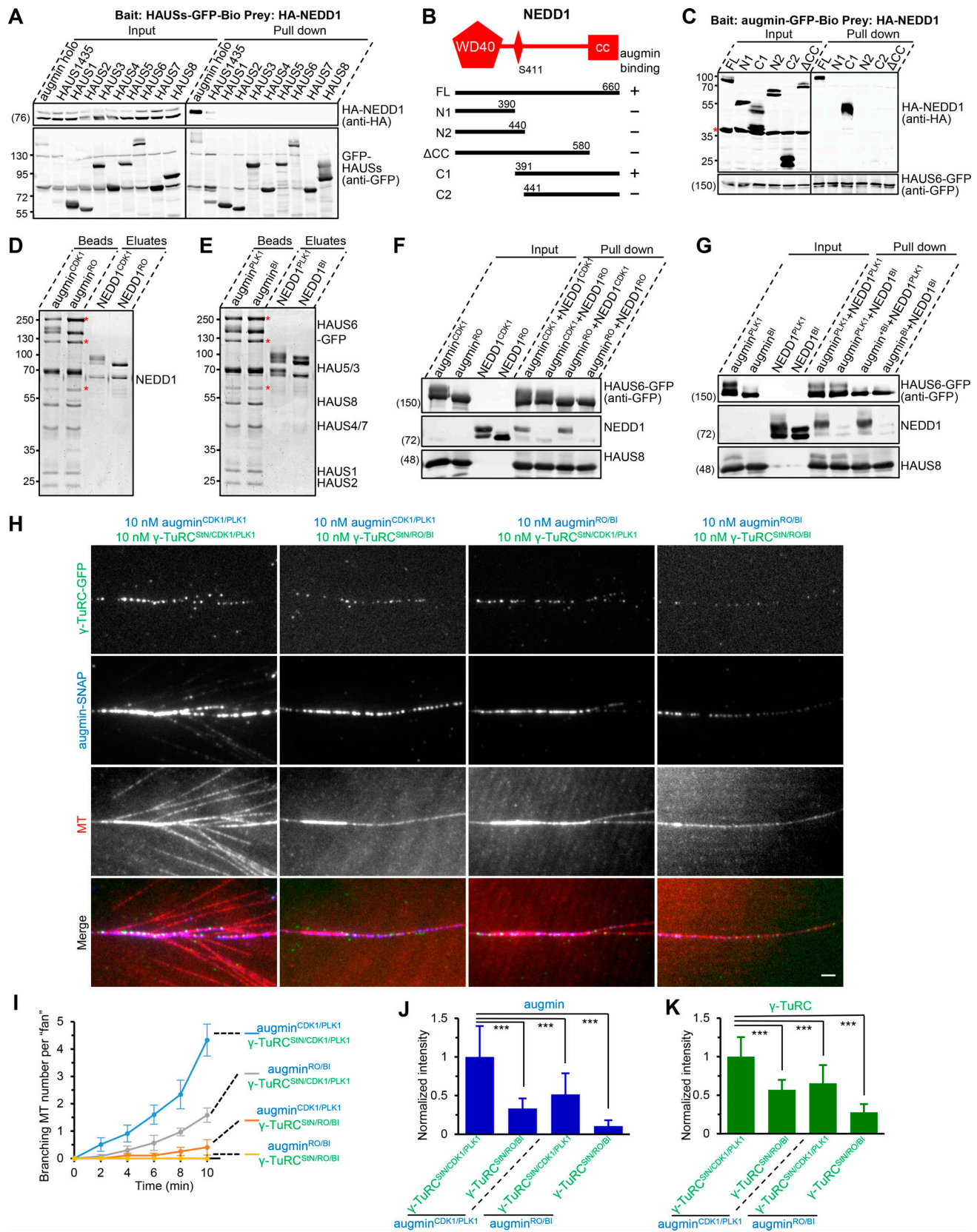


Figure 6. **Biochemical characterization of phosphorylation-dependent NEDD1-augmin interaction and branching MT nucleation.** (A) Streptavidin pull-down assay with extracts of nocodazole-arrested mitotic HEK293T cells expressing HA-NEDD1 (prey) together with Bio-GFP-tagged augmin holo complex, H1/H4/H3/H5 subcomplex, or eight individual subunits (bait), analyzed by Western blotting with indicated antibodies. (B) Schematic overview of the domain organization of NEDD1 and the deletion mutants, and summary of their interactions with augmin. N, N-terminus; C, C-terminus. (C) Streptavidin pull-down

assay with extracts of nocodazole-arrested mitotic HEK293T cells expressing Bio-GFP-tagged augmin holo complex (bait) together with HA-tagged NEDD1 or its indicated fragments (prey), analyzed by Western blotting with indicated antibodies. Asterisk indicates the bands of HA-BirA, which was cotransfected for biotinylating bait proteins. **(D and E)** Coomassie blue-stained gels with flag-NEDD1 and augmin-GFP-Strep purified from nocodazole-arrested mitotic HEK293T cells in the presence of either coexpressed untagged CDK1/cyclin B, HA-PLK1, or individual inhibitors. Asterisks indicate endogenous biotinylated proteins that were captured by StrepTactin beads during purification. **(F and G)** StrepTactin pull-down assays using indicated versions of augmin-GFP-Strep immobilized on StrepTactin beads as the bait and indicated versions of flag-NEDD1 eluates as the prey, analyzed by Western blotting with indicated antibodies. **(H)** TIRF microscopy images of branching MT nucleation in the presence of indicated pairs of 10 nM augmin-SNAP (blue) and 10 nM γ -TuRC-GFP^{S_{1N}} (green). Images were acquired 10 min after imaging. **(I)** Quantification of the total number of branched MTs per fan-like structure at indicated time points in the assays performed with indicated pairs of complexes. $n = 3$ experiments. **(J and K)** Quantification of intensities of augmin-SNAP (J) and γ -TuRC-GFP^{S_{1N}} (K) along MTs for the experiments shown in H. The values were normalized to the intensity of the pair of augmin^{CDK1/PLK1} and γ -TuRC^{S_{1N}/CDK1/PLK1}. $n = 50$ MTs from three experiments. Scale bars, 2 μ m. Data represent mean \pm SD. ***, $P < 0.001$, two-tailed t test.

phosphorylation by CDK1/PLK1 are required. In addition, we observed that the augmin^{CDK1/PLK1}- γ -TuRC^{S_{1N}/CDK1/PLK1} pair resulted in dramatically increased intensities of each other along MTs compared to other pairs (Fig. 6, J and K), suggesting that a phosphorylation-dependent synergy exists between MT-binding activities of augmin and γ -TuRC.

We next investigated what would happen to the branching efficiency if γ -TuRC was prepared using different strategies. One strategy was to use the constructs with GCP3 tagged with Strep (see also Fig. S3 C) and coexpress them with kinases. To differentiate this resulting complex from γ -TuRC^{S_{1N}/CDK1/PLK1} mentioned above, we referred to it as γ -TuRC^{G3St/CDK1/PLK1} (G3 is short for GCP3). Another strategy was to prepare a version of phosphorylated γ -TuRC that lacks NEDD1 subunit (termed as γ -TuRC ^{Δ N/G3St/CDK1/PLK1}). The nucleation activities of these different versions of γ -TuRC (all at 10 nM) were first compared; the strongest activity was observed for γ -TuRC^{S_{1N}/CDK1/PLK1}, lower for γ -TuRC^{G3St/CDK1/PLK1} (~64% that of γ -TuRC^{S_{1N}/CDK1/PLK1}), and the lowest for γ -TuRC ^{Δ N/G3St/CDK1/PLK1} (~26% that of γ -TuRC^{S_{1N}/CDK1/PLK1}; Fig. 7, A and B). These different versions of γ -TuRC were further evaluated in the presence of augmin. Although the augmin^{CDK1/PLK1}- γ -TuRC^{G3St/CDK1/PLK1} pair (10 nM augmin; 10 nM γ -TuRC) could also induce branching nucleation, the branching nucleation activity of this pair was only ~15% that of the augmin^{CDK1/PLK1}- γ -TuRC^{S_{1N}/CDK1/PLK1} pair (10 nM augmin; 10 nM γ -TuRC; Fig. 7, A and E). The differences in nucleation activity between γ -TuRC^{S_{1N}/CDK1/PLK1} and γ -TuRC^{G3St/CDK1/PLK1} could only partly account for the striking differences in branching efficiency. Another reason is that the stoichiometry of NEDD1, the adaptor protein within the branching machinery, was much lower in γ -TuRC^{G3St/CDK1/PLK1} than that in γ -TuRC^{S_{1N}/CDK1/PLK1} (Fig. 7 C). As expected, γ -TuRC ^{Δ N/G3St/CDK1/PLK1} combined with augmin^{CDK1/PLK1} failed to induce branching nucleation; however, this could be rescued by add-back of the separately purified NEDD1 in phosphorylated form (termed as NEDD1^{CDK1/PLK1}; Fig. 7, A, D, and E). Surprisingly, the branching nucleation activity peaked at a moderate concentration (10 nM; ~76% that of the augmin^{CDK1/PLK1}- γ -TuRC^{S_{1N}/CDK1/PLK1} pair) and dropped at a high concentration (20 nM) of NEDD1 (Fig. 7, D and E). Although we cannot exclude other possibilities, we reason that at high NEDD1 concentrations, an excess of free NEDD1 could sequester augmin, preventing it from binding to γ -TuRC. Because the γ -TuRC^{S_{1N}/CDK1/PLK1} approach proved to be the most effective, in subsequent experiments, γ -TuRC was prepared in this way.

We then tested the effect of CDK1 and PLK1 inhibition on the localization of γ -TuRC and augmin in cells. Consistent with previous results (Haren et al., 2009; Zhu et al., 2009), PLK1 inhibition with BI2536 resulted in reduced spindle localization of both augmin and γ -TuRC (Fig. S4, G–J). A similar reduction was observed upon inhibition of CDK1 with RO3306 (Fig. S4, K–N). Taken together, these data demonstrate that both phosphorylation of γ -TuRC and augmin by CDK1 and PLK1 are necessary for the branching nucleation and for their synergistic MT-binding activities.

Augmin is not only a recruiting factor but also an activator of γ -TuRC

Previous work using purified *Drosophila* proteins has shown that augmin can stimulate γ -TuRC-dependent nucleation in vitro; however, studies using *Xenopus* proteins reported contradictory findings. We then investigated this issue in our in vitro system. The nucleation activity of γ -TuRC (γ -TuRC^{S_{1N}/CDK1/PLK1}) was evaluated over a range of concentrations from 1 to 10 nM in the absence or presence of a fixed concentration of augmin (augmin^{CDK1/PLK1}; 10 nM). The addition of augmin enhanced overall γ -TuRC-dependent MT nucleation at all tested concentrations (1.3-, 5.3-, and 6.2-fold at 1, 5, and 10 nM, respectively; Fig. 7, F and G). This enhancement mainly originated from the MT lattice-bound pool of γ -TuRC rather than γ -TuRC in solution (Fig. 7 H). Therefore, augmin could augment γ -TuRC-dependent MT nucleation by recruiting and specifically activating it on lattice.

NEDD1 WD40 domain confers MT-binding activity and is essential for branching nucleation

We then focused on investigating NEDD1 behavior in vitro, as it is the direct point of contact between γ -TuRC and augmin. Interestingly, we found that NEDD1 exhibited MT binding activity, and its accumulation along MTs increased with increasing concentrations (Fig. 8, A and B). Furthermore, the WD40 domain of NEDD1 (WD) could bind MTs, albeit with much lower affinity than the full-length protein, whereas the fragment lacking the WD40 domain (Δ WD) displayed no MT binding. The fragment Δ CC, which contains both WD and linker but lacks the C-terminal CC domain, showed similar binding to MTs as WD. Fusion with the leucine zipper from GCN4 (LZ) can increase Δ CC's binding for MTs; however, this binding was still below that of the full-length protein, suggesting that the higher MT-binding affinity of full-length NEDD1 than WD is not merely a

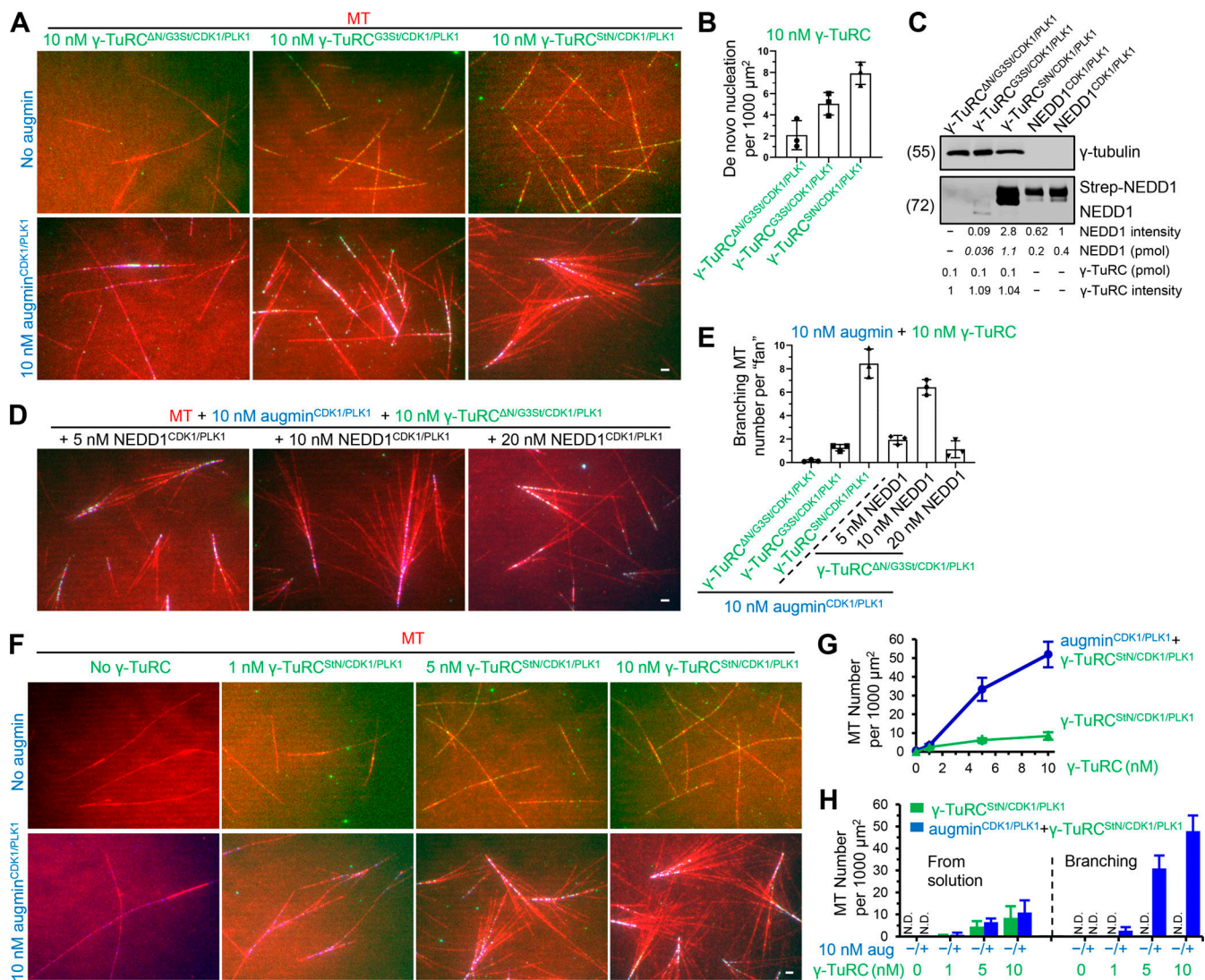


Figure 7. Evaluation of different versions of γ -TuRC in the absence or presence of augmin. (A) TIRF microscopy images of MTs (red) grown in the presence of 10 nM indicated versions of γ -TuRC (green) together with (lower panels) or without (upper panels) 10 nM augmin-SNAP (blue). (B) Quantification of de novo nucleation of MTs from solution for experiments shown in upper panels of A. $n = 3$ experiments. (C) Western blot analysis of 0.1 pmol indicated versions of γ -TuRC-GFP as well as 0.2 and 0.4 pmol Strep-NEDD1^{CDK1/PLK1} with γ -tubulin and NEDD1 antibodies. The amounts of NEDD1 in indicated versions of γ -TuRC-GFP were estimated by comparing their band intensities with those of defined quantities of NEDD1 proteins. (D) TIRF microscopy images of branching MT nucleation in the presence of 10 nM augmin^{CDK1/PLK1}-SNAP (blue) and 10 nM γ -TuRC ^{Δ N/G3S1/CDK1/PLK1}-GFP (green) together with Strep-NEDD1^{CDK1/PLK1} (dark) at indicated concentrations. (E) Quantification of the total number of branched MTs per fan-like structure for experiments shown in D and lower panels of A. $n = 3$ experiments. (F) TIRF microscopy images of MTs (red) grown in the presence of γ -TuRC^{S1N/CDK1/PLK1}-GFP at indicated concentrations together with (lower panels) or without (upper panels) 10 nM augmin^{CDK1/PLK1}-SNAP (blue). (G) Quantification of the overall γ -TuRC-dependent nucleation of MTs for experiments shown in F. $n = 3$ experiments. (H) Quantification of MTs originated from γ -TuRC in solution (left of dashed line) or lattice-bound pool of γ -TuRC (right of dashed line; branching nucleation) for experiments shown in F. $n = 3$ experiments. Scale bar, 2 μ m. Data represent mean \pm SD.

consequence of dimerization (Fig. 8, C-E). These results were unexpected, because a previous study using bacterially expressed *Xenopus* NEDD1 proteins showed that a truncation mutant lacking the WD40 domain was able to bundle MTs in vitro, while the full-length protein or WD40 domain failed to do so (Liu and Wiese, 2008). Taken together, these data demonstrate that WD is the minimal region necessary for NEDD1's MT-binding activity.

We then set out to determine the contribution of NEDD1 WD in branching nucleation. Strep-tagged NEDD1 Δ WD could co-purify with other subunits of γ -TuRC like that of full-length

NEDD1, and this resulting complex was referred to as γ -TuRC ^{Δ WD/S1N/CDK1/PLK1}. The NEDD1 Δ WD/ γ -TuRC molar ratio in γ -TuRC ^{Δ WD/S1N/CDK1/PLK1} was lower than the NEDD1/ γ -TuRC molar ratio in WT γ -TuRC^{S1N/CDK1/PLK1} (10:1 versus 15:1). γ -TuRC ^{Δ WD/S1N/CDK1/PLK1} displayed a dramatic reduction in MT binding (\sim 21% at 10 nM; \sim 13% at 50 nM) but preserved roughly half of the nucleation activity in solution (Fig. S5, A-D). Nonetheless, in contrast to the WT γ -TuRC^{S1N/CDK1/PLK1}, 10 nM of which in complex with 10 nM augmin^{CDK1/PLK1} was sufficient to stimulate branching nucleation, γ -TuRC ^{Δ WD/S1N/CDK1/PLK1} at the same concentration failed to do so. Even at a 10-fold higher

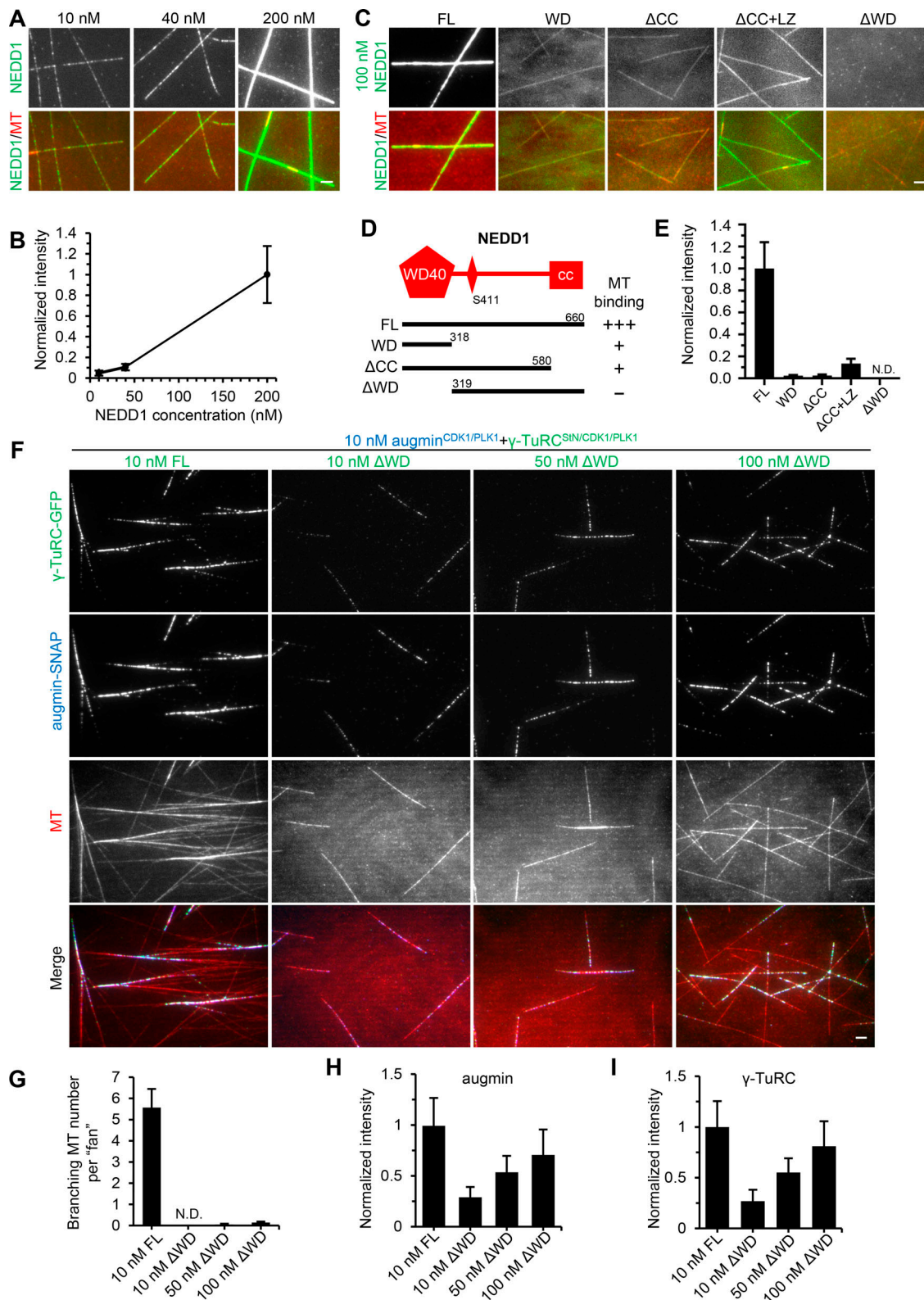


Figure 8. **NEDD1 WD40 domain possesses MT-binding activity and is essential for branching nucleation.** (A and B) TIRF microscopy images and quantification of NEDD1-GFP (green) binding at indicated concentrations to MTs (red). The values were normalized to the intensity of 200 nM NEDD1-GFP. $n = 30$ MTs from two experiments. (C and E) TIRF microscopy images and quantification of the binding of 100 nM C-terminally GFP-tagged NEDD1 or its indicated fragments (green) to MTs (red). The values were normalized to the intensity of full-length (FL) NEDD1-GFP. $n = 30$ MTs from two experiments. (D) Schematic overview of the domain organization of NEDD1 and the deletion mutants, and summary of their MT binding activity. (F) TIRF microscopy images of branching MT nucleation in the presence of 10 nM augmin^{CDK1/PLK1}-SNAP (blue) together with 10 nM γ -TuRC^{SIN/CDK1/PLK1}-GFP or indicated concentrations of γ -TuRC^{ΔWD/SIN/CDK1/PLK1}-GFP (green). Images were acquired 10 min after imaging. (G) Quantification of the total number of branched MTs per fan-like structure

for the experiments shown in F. N.D., not detected. $n = 3$ experiments. **(H and I)** Quantification of intensities of augmin^{CDK1/PLK1}-SNAP (H) and γ -TuRC^{S^{5N}/CDK1/PLK1}-GFP or γ -TuRC ^{Δ WD/S^{5N}/CDK1/PLK1}-GFP (I) along MTs for the experiments shown in F. The values were normalized to the intensity of the pair of 10 nM augmin^{CDK1/PLK1} and 10 nM γ -TuRC^{S^{5N}/CDK1/PLK1}. $n = 60$ MTs from three experiments. Scale bars, 2 μ m. Data represent mean \pm SD.

concentration (100 nM), at which concentration γ -TuRC ^{Δ WD/S^{5N}/CDK1/PLK1} intensity along MTs was comparable to that of the WT γ -TuRC^{S^{5N}/CDK1/PLK1} at 10 nM, only rare branching nucleation events were observed (Fig. 8, F-I; and Video 10). These data demonstrate that NEDD1 WD is essential for branching nucleation and suggest that it not only confers MT binding affinity but also involves in activation of branching nucleation.

Different roles for NEDD1 phosphorylation and augmin phosphorylation in their synergistic MT-binding activities

As it was demonstrated above that the combination of augmin and γ -TuRC, both in phosphorylated forms, strongly enhanced each other's accumulation along MTs, we wondered whether NEDD1 could account, on its own, for the contribution of γ -TuRC in this synergistic increase. Therefore, purified NEDD1 and augmin in either phosphorylated or nonphosphorylated form (NEDD1^{CDK1/PLK1} versus NEDD1^{RO/BI}; augmin^{CDK1/PLK1} versus augmin^{RO/BI}) were first individually applied to the in vitro assay at various concentrations. By measuring their intensities along the MTs and comparing the phosphorylated versus non-phosphorylated forms at the same concentration, we found that phosphorylation by PLK1 and CDK1 led to a significant increase for augmin but a dramatic decrease for NEDD1 in MT-binding activity. Side-by-side analysis of augmin^{CDK1/PLK1} and NEDD1^{CDK1/PLK1} revealed that augmin^{CDK1/PLK1} intensity along MTs was \sim 20-fold higher than that of NEDD1^{CDK1/PLK1} (Fig. 9, A, B, and D).

Next, we investigated four pairs of augmin and NEDD1, in either phosphorylated or nonphosphorylated form. Quantification analyses revealed that the augmin^{CDK1/PLK1}-NEDD1^{CDK1/PLK1} pair was the most potent to boost each other's intensities along MTs, whereas the augmin^{CDK1/PLK1}-NEDD1^{RO/BI} pair and the augmin^{RO/BI}-NEDD1^{CDK1/PLK1} pair were less potent, and the augmin^{RO/BI}-NEDD1^{RO/BI} pair was the least potent (Fig. 9, C, E, and F), consistent with the trend of branching efficiency and MT binding intensities exhibited by four pairs of augmin and γ -TuRC with different phosphorylation states (Fig. 6, H-K). These data demonstrate that NEDD1 is indeed the functionally critical component of γ -TuRC to the synergy and that the synergistic effect of augmin and NEDD1 on their MT binding activity requires them both in phosphorylated forms. The requirement for augmin phosphorylation may reflect its enhanced MT-binding activity and hence the stronger recruitment of NEDD1, while the requirement for NEDD1 phosphorylation may reflect its importance in the formation of the complete complex and therefore indicate that the synergy depends on direct interaction. However, phosphorylation of NEDD1, in fact, reduced its own MT-binding activity. This raises the question of whether NEDD1's intrinsic affinity for MTs is dispensable for this synergy? To address this, we resorted to NEDD1 Δ WD, which lacks the MT-binding domain. We found that although the

augmin^{CDK1/PLK1}-NEDD1 Δ WD^{CDK1/PLK1} pair could enhance each other's accumulation along MTs, their intensities along MTs were much lower than that observed in the augmin^{CDK1/PLK1}-NEDD1^{CDK1/PLK1} pair (Fig. S5, E-H), indicating that even though the MT-binding activity conferred by NEDD1 WD40 domain is negatively regulated by phosphorylation, the presence of WD40 domain is still necessary for a robust synergy. Collectively, we conclude that the observed synergy between augmin and NEDD1 depends on CDK1- and PLK1-dependent phosphorylation of them both and that the MT-binding domain of NEDD1 could contribute to the synergy.

Discussion

In this study, using purified components from both native and recombinant sources, we demonstrate that human augmin and γ -TuRC are sufficient to reconstitute the minimal MT branching machinery, the assembly and activity of which require CDK1- and PLK1-mediated phosphorylation in a cell cycle-dependent manner (Fig. 9 G). Our reconstitution system allows real-time observation of both augmin and γ -TuRC behavior during branching nucleation and quantitative definition of the branching events. In addition, we unveil that as a bridging factor, NEDD1 directly binds to the augmin holo complex and MZT1/GCP3 NTE subcomplex of γ -TuRC. Importantly, its N-terminal WD40 domain confers an MT-binding activity to NEDD1, which plays an essential role in activating branching nucleation.

In our in vitro system, human augmin and γ -TuRC are necessary and sufficient to initiate robust branching MT nucleation, similar to that observed in *Drosophila* but contrasting with reports in *Xenopus*, where TPX2 is required. This discrepancy may stem from mechanistic differences in branching pathways across species or different methodologies applied to prepare the core components. Nevertheless, we cannot exclude the possibility that in human cells, TPX2 can still facilitate branching MT nucleation through an indirect mechanism by stabilizing freshly nucleated nascent MTs and counteracting catastrophe factors. Of note, TPX2 and other reported binding partners of γ -TuRC, such as CEP192, CDK5RAP2, AKAP9, Pericentrin, and ch-TOG (Takahashi et al., 2002; Choi et al., 2010; Joukov et al., 2014; Thawani et al., 2018), were not detected in the mass spectrometry analysis of γ -TuRC (which was purified using low-salt buffer; Table S1 F), maybe owing to the low binding affinity.

Our reconstitution assay makes it possible to visualize and analyze the behavior of both augmin and γ -TuRC during the process of branching nucleation for the first time in vitro. The steps of a branching nucleation event directly observed in *Drosophila* cells and postulated in plant cells entail augmin binding first to the mother MT, followed by recruitment of γ -TuRC, and subsequent nucleation of the daughter MT at a branch angle (Liu et al., 2014b; Verma and Maresca, 2019). However, most branching events observed in our in vitro assays involve

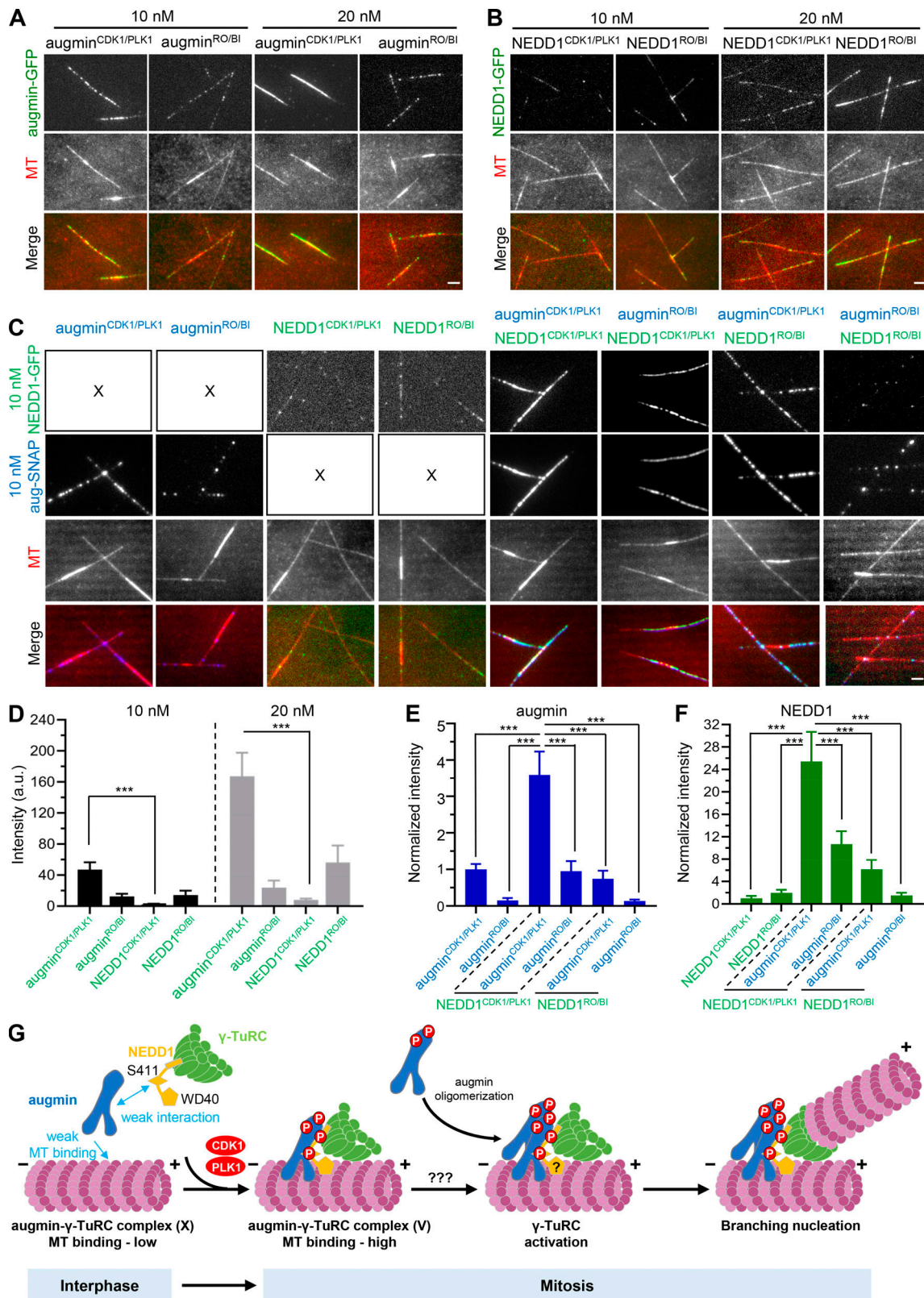


Figure 9. **Different roles for NEDD1 phosphorylation and augmin phosphorylation in their synergistic MT-binding activities.** (A and B) TIRF microscopy images of MTs (red) grown in the presence of augmin^{CDK1/PLK1}-GFP, augmin^{RO/BI}-GFP, NEDD1^{CDK1/PLK1}-GFP, or NEDD1^{RO/BI}-GFP (green) at indicated concentrations. (C) TIRF microscopy images of MTs (red) grown in the presence of different versions of 10 nM augmin-SNAP (blue; augmin^{CDK1/PLK1} and augmin^{RO/BI}) and 10 nM NEDD1-GFP (green; NEDD1^{CDK1/PLK1} and NEDD1^{RO/BI}), either alone or combined in pairs. (D) Quantification of intensities of indicated versions of augmin and NEDD1 along MTs for the experiments shown in A and B. *n* = 60 MTs from three experiments. (E and F) Quantification of intensities of indicated versions of augmin-SNAP (E) and NEDD1-GFP (F) along MTs for the experiments shown in C. The values were normalized to the intensity of

augmin^{CDK1/PLK1}-SNAP alone (E) or NEDD1^{CDK1/PLK1}-GFP alone (F). $n = 40$ MTs from three experiments. (G) Model for cell cycle-dependent regulation of branching MT nucleation. In interphase, the interaction between augmin and γ -TuRC is weak, and the MT-binding affinity of augmin is also low. Therefore, branching MT nucleation does not occur at this stage in the human system. Upon entry into mitosis, CDK1- and PLK1-mediated phosphorylation drives the formation of a stable MT branching machinery, the complete augmin- γ -TuRC complex, and promotes a synergistic enhancement of the MT-binding activity of this machinery. NEDD1 WD40 domain plays an essential role in activating the branching nucleation via a yet unknown mechanism. Augmin oligomerization may also play an important role in the activation step. Scale bars, 2 μ m. Data represent mean \pm SD. ***, $P < 0.001$, two-tailed t test.

simultaneous binding of augmin and γ -TuRC. A simple explanation for this discrepancy is that augmin and γ -TuRC already form a complex during our copurification procedure, while a stable complex cannot form in the cytoplasm of *Drosophila* and plant cells, and the binding of augmin to MT may favor its association with γ -TuRC. Consistent with previous results (Liu et al., 2014b; Verma and Maresca, 2019), in our assays, there is also a lag time between γ -TuRC binding and branching nucleation, which we assume to be the activation step. Interestingly, we found that during this lag time, the γ -TuRC intensity remains largely unchanged, while augmin intensity progressively increases over time, suggesting that oligomerization of augmin may play an important role in the activation of the nucleator γ -TuRC. In addition, the small branch angles ($<30^\circ$ for $\sim 77\%$ branching events) we observed here are similar to those measured in *Xenopus* egg extracts (Petry et al., 2013), observed by electron tomography of the spindle of human U2OS cells in metaphase (Kamasaki et al., 2013), suggesting that our in vitro system can recapitulate the physiological properties of branching MT nucleation.

We demonstrate that via its C-terminal CC domain, NEDD1 specifically binds to the γ -TuRC subcomplex formed by MZT1 and N-terminal extension of GCP3. Furthermore, recent cryo-EM structures reveal that γ -TuRC exhibits an asymmetric and conical structure, with GCP3 being located at positions 2, 4, 6, 8, and 14. Accordingly, only these positions, which occupy the half side of the cone-shaped γ -TuRC, can provide binding sites for NEDD1 (Fig. 5 I). Therefore, we speculate that as a factor bridging the augmin- γ -TuRC complex, NEDD1's asymmetric arrangement may confer directionality to this branching machinery. Moreover, via its WD40 domain, NEDD1 binds to MTs, and the absence of this domain abolishes the branching nucleation activity. Currently, it is difficult to dissect the mechanism underlying the role of the WD40 domain in the activation of the branching nucleation. We envisage that the simultaneous binding of augmin and NEDD1 WD40 domain to the sidewall of preexisting MTs may orient γ -TuRC in a branching nucleation-competent conformation (Fig. 9 G).

Using purified recombinant proteins, we showed that augmin exhibits time-dependent accumulation along MTs in vitro, likely due to oligomerization. Consequently, it displays older GDP-MT region bias, which may further explain the biased distribution pattern of branching sites. Consistent with this property of augmin, a recent functional study through a combination of live imaging and mathematical modeling showed that accumulation of augmin on long-lived MTs can drive the assembly of kinetochore-fiber in human cells (David et al., 2019).

The strategy of multigene expression in HEK293T cells makes it possible to manipulate posttranslational modifications of large

protein complexes, which provides a basis for the mechanistic understanding of the respective contribution of augmin phosphorylation and γ -TuRC phosphorylation to the branching nucleation. In addition, the copurification strategy we developed here to isolate the recombinant complete augmin- γ -TuRC complex could be applied to future structural studies of this branching machinery.

Materials and methods

DNA constructs

The subunits of human augmin complex, HAUS1 (NM_138443.4), HAUS2 (NM_018097.3), HAUS3 (NM_001303143.2), HAUS4 (NM_001166269.2), HAUS5 (NM_015302.2), HAUS6 (NM_017645.5), HAUS7 (NM_001385482.1), and HAUS8 (NM_033417.2); human γ -TuRC subunits, γ -tubulin (NM_001070.5), GCP2 (NM_006659.4), GCP3 (NM_006322.6), GCP4 (NM_014444.5), GCP5 (NM_052903.6), GCP6 (NM_020461.4), MZT1 (NM_001071775.3), MZT2A (NM_001085365.2), MZT2B (NM_025029.5), NEDD1 (NM_001135176.2), and NME7 (NM_013330.5); and the kinases PLK1 (NM_005030.6) and CDK1 (NM_001786.5)/cyclin B (NM_031966.4) used in this study were amplified from HeLa cDNA. The genes described above were cloned into pTT5Multi, pTT5-GFP-Strep N1/mCherry-Strep N1/SNAP-Strep N1/Strep N1/Strep C1, pTT5-3*HA-C1, pTT5-3*Flag-C1, Bio-C1, Bio-GFP-C1, GFP-Bio-N1 vectors.

Multigene-expression DNA constructs

Construction of the pTT5Multi vector for coexpression of multiple proteins

To construct the pTT5Multi vector, the Orip element was first removed from the previously described plasmid pTT5 Strep-GFP C1 (Hua and Jiang, 2020). Three restriction enzyme sites for AvrII, MluI, and AscI were inserted after the poly(A) sequence to give rise to the plasmid pTT5Multi Strep-GFP C1. Finally, pTT5Multi Strep-GFP C1 was digested by NheI and BspEI and ligated with the annealing product of two primers (forward: 5'-CTAGCGCCACCGGCGGCAGTGGCGGCT-3'; reverse: 5'-CCGGAGCCGCCACTGCCCGGTGGCG-3'). The resulting plasmid was named pTT5Multi vector, containing a CMV5 promoter, multiple cloning sites (MCSs), and a poly(A) terminator. Note that SpeI, AvrII, and MluI are three important restriction sites for the cloning strategy (see Fig. S3 A).

Then, construction of the pTT5Multi plasmid that contains multiple gene cassettes was performed as follows (see Fig. S3 B). First, Gene1 and Gene2 were individually cloned into the MCS of the empty pTT5Multi vector, generating two plasmids, pTT5Multi-Gene1 and pTT5Multi-Gene2. Then, pTT5Multi-Gene1 was double digested with AvrII and MluI, while

pTT5Multi-Gene2 was double digested with SpeI and MluI. As AvrII and SpeI were isocaudomers, after double digestion, the backbone containing Gene1 cassette was ligated with the fragment containing Gene2 cassette to give rise to the plasmid pTT5Multi-Gene1-Gene2. Since the plasmid pTT5Multi-Gene1-Gene2 still contains the SpeI, AvrII, and MluI sites, this process can be repeated to add more gene cassettes. Of note, if the genes of interest happen to contain the MluI sites, the AscI site of the pTT5Multi vector could be used to replace the MluI site, as MluI and AscI were also isocaudomers.

pTT5Multi vector-based plasmids used in this study

Using the strategy described above, for recombinant augmin complex, pTT5Multi-HAUS6-tag/HAUS2, pTT5Multi-HAUS8/HAUS3, pTT5Multi-HAUS7/HAUS5, and pTT5Multi-HAUS4/HAUS1 were first assembled and then further assembled into the final two plasmids, pTT5Multi-HAUS6-tag/HAUS2/HAUS8/HAUS3 and pTT5Multi-HAUS7/HAUS5/HAUS4/HAUS1. Tags for augmin in this study: GFP-Strep, mCherry-Strep, SNAP-Strep, and GFP-Bio.

Similarly, for recombinant γ -TuRC and γ -TuRC^{G3St} in Figs. 3, 4, 7, and S3, the following plasmids were used: pTT5Multi-GCP3-GFP-(Strep)/GCP2/ γ -tubulin/ γ -tubulin, pTT5Multi-GCP4/GCP6/GCP5, and pTT5Multi-MZT2A/MZT2B/MZT1/NME7/NEDD1; Strep-tag was present when γ -TuRC was separately purified (Fig. 3, F and G; Fig. 7, A and D; and Fig. S3 F) and was absent when γ -TuRC was copurified with augmin complex (Figs. 3 H, 4 E, and S3 L). For recombinant γ -TuRC^{SIN} and γ -TuRC ^{Δ WD/SIN} in Fig. 6 H; Fig. 7, A and F; and Figs. 8 F, S4 F, and S5 B, pTT5Multi-GCP3-GFP/GCP2/ γ -tubulin/ γ -tubulin, pTT5Multi-GCP4/GCP6/GCP5, and pTT5Multi-MZT2A/MZT2B/MZT1/NME7 together with pTT5-Strep-NEDD1 or pTT5-Strep-NEDD1 Δ WD were used. For recombinant γ -TuRC ^{Δ N/G3St} in Fig. 7, A and D, pTT5Multi-GCP3-GFP-Strep/GCP2/ γ -tubulin/ γ -tubulin, pTT5Multi-GCP4/GCP6/GCP5, and pTT5Multi-MZT2A/MZT2B/MZT1/NME7 were used. The γ -tubulin subunit has two copies to achieve higher expression levels. In addition, pTT5Multi-cyclin B/CDK1 and pTT5Multi-Strep-cyclin B/CDK1 were made to express the CDK1/cyclin B complex.

Cell culture and transfection

Human HEK293T and HeLa cells were maintained in DMEM/F12 (1:1) medium supplemented with 10% FBS, 5 U/ml penicillin, and 50 μ g/ml streptomycin and incubated at 37°C under 5% CO₂ humidified atmosphere. FuGENE6 (Promega) was used to transfect HeLa cells for knock-in experiments. Polyethylenimine (Polysciences) was used to transfect HEK293T cells for protein purification and pull-down experiments.

PLK1 inhibitor BI2536 (TargetMol), CDK1 inhibitor RO3306 (TargetMol), S-trityl-L-cysteine (STLC; TargetMol), and nocodazole (Sigma-Aldrich) were dissolved in sterile DMSO as stock solutions according to the manufacturer's instructions and kept at -20°C. HEK293T cells or HeLa knock-in cells were treated with 200 ng/ml nocodazole for ~16 h before harvesting to arrest cells in mitosis for purification and pull-down experiments. For immunofluorescence experiments, before fixation, cells were treated with 10 μ M RO3306 for 30 min or with 100 μ M STLC for 4 h; in the combined treatment, 300 nM BI2536 was added into medium for the last 2 h of incubation with STLC. For pull-down

assays, cells were treated with 5 μ M RO3306 or 300 nM BI2536 for indicated time periods.

Antibodies

The following primary antibodies were used: rabbit polyclonal antibodies against HAUS1 (11094-2-AP, Western blot [WB]-1:1,000; Proteintech), HAUS2 (A13707, WB-1:1,000; Abclonal), HAUS3 (18991-1-AP, WB-1:1,000; Proteintech), HAUS4 (20104-1-AP, WB-1:1,000; Proteintech), HAUS6 (16933-1-AP, WB-1:1,000; Proteintech), HAUS7 (17830-1-AP, WB-1:1,000; Proteintech), HAUS8 (A7847, WB-1:1,000, IF-1:300; Abclonal), GFP (50430-2-AP, WB-1:1,000; Proteintech), and SNAP (A00684, immunofluorescence [IF]-1:300; GenScript); mouse polyclonal antibodies against HA (51064-2-AP, WB-1:1,000; Proteintech); mouse monoclonal antibodies against NEDD1 (SC-100961, WB-1:1,000, IF-1:300; Santa Cruz), γ -tubulin (MA1-19421, WB-1:1,000, IF-1:600; Thermo Fisher Scientific), GCP2 (SC-377117, WB-1:1,000; Santa Cruz), GCP3 (SC-373758, WB-1:1,000; Santa Cruz), GCP6 (SC-374063, WB-1:1,000; Santa Cruz), and a rat monoclonal antibody against α -tubulin YL1/2 (MA1-80017, IF-1:600; Thermo Fisher Scientific).

Generation of stable cell lines

The knock-in cell lines were generated using CRISPR/Cas9 technology. sgRNA and Cas9 were expressed in PX459 (#62988; Addgene). Gibson assembly was used to assemble the pUC19-based GFP-Strep and SNAP donor plasmids.

To tag HAUS8 locus with GFP-Strep at the C-terminus, HeLa cells seeded on a 6-well plate were cotransfected with 2 μ g donor construct harboring the GFP-Strep cassette (5' homology-arm forward, 5'-GTGGTTTTGCCATGTTGCCCA-3'; 5' homology-arm reverse, 5'-TGACAAGTCCCCTCCCTGAACGAGAG-3'; 3' homology-arm forward, 5'-CTCATGGTTACATTACAGGATACTTGAGCACT-3'; 3' homology-arm reverse, 5'-AAGTCCCAGTGGAGCACAGATG-3') and 1 μ g PX459 bearing sgRNA (gRNA: 5'-GAGGGACTTGTGACTGACTCA-3'). 24 h after transfection, cells were selected with 8 μ g/ml puromycin for 2 d. 3 d after removal of puromycin, single-cell cloning was performed by serial dilution. Positive knock-in clones were screened by fluorescence microscopy and further verified by Western blotting and PCR genotyping (5'-CACGCCCTGTCTGAGGACG-3' and 5'-GAGCCAGTCGGGTAAAAGTGG-3').

To tag GCP2 locus with SNAP at the C-terminus, HAUS8-GFP-Strep knock-in HeLa cells seeded on a 6-well plate were cotransfected with 2 μ g donor construct harboring the SNAP cassette (5' homology-arm forward, 5'-ACCTGTCCCTGCATCCA GGC-3'; 5' homology-arm reverse, 5'-CTGTGCGGTGACTGCGAC-3'; 3' homology-arm forward, 5'-GCCCTGGCTGTGACAGGAAG-3'; 3' homology-arm reverse, 5'-AACCTTTGTTCCCGCAGG-3') and 1 μ g PX459 bearing sgRNA (gRNA: 5'-AGTCACCGCACAGTGAGCCC-3'). Subsequent steps were performed in a similar manner as described above (PCR genotyping primers: 5'-TTCAATGGTTTCTACACGGA-3' and 5'-ACAACCTCCCTGACCGTTTC-3').

Protein expression and purification

Purification of native augmin- γ -TuRC complex

For native augmin- γ -TuRC complex used in Figs. 1 and 2, six 15-cm dishes of HAUS8-GFP-Strep knock-in or HAUS8-GFP-Strep/

GCP2-SNAP double knock-in HeLa cells at ~80% confluence were treated with 200 ng/ml nocodazole for 16 h before harvesting. After the medium was removed, cells were collected with cold PBS (10 ml for each dish), followed by centrifugation at 1,000 rpm for 5 min. Then total cell pellets were lysed in 6 ml lysis buffer (50 mM Hepes, 150 mM NaCl, 1 mM EGTA, 1 mM MgCl₂, 0.5% Triton X-100, 0.1 mM GTP, and 1 mM DTT, pH 7.4) containing EDTA-free protease inhibitors (Roche) for 10 min on ice. After centrifugation at 14,000 rpm for 20 min, the supernatant was incubated with 100 μl StrepTactin Sepharose beads (GE Healthcare) at 4°C for 45 min. After removing the supernatant by centrifuging at 3,000 rpm, 4°C for 1 min, beads were washed four times with 1 ml lysis buffer and twice with 1 ml wash buffer A (50 mM Hepes, 150 mM NaCl, 1 mM EGTA, 1 mM MgCl₂, 0.01% Triton X-100, 0.1 mM GTP, 1 mM DTT, pH 7.4) by inverting the tube four to six times. Subsequently, in the case of HAUS8-GFP-Strep knock-in, proteins were eluted with 60 μl elution buffer (50 mM Hepes, 150 mM NaCl, 1 mM EGTA, 1 mM MgCl₂, 0.01% Triton X-100, 0.1 mM GTP, 1 mM DTT, and 2.5 mM desthiobiotin, pH 7.4), while in the case of HAUS8-GFP-Strep/GCP2-SNAP double knock-in, to label SNAP-tagged GCP2, beads were incubated with 100 μl wash buffer A containing 10 μM SNAP-Surface Alexa Fluor 647 (NEB) at 4°C in darkness for 1 h, followed by washing four times with 1 ml lysis buffer and twice with 1 ml wash buffer A by inverting the tube four to six times and the final elution step with 60 μl elution buffer. All purified proteins were snap-frozen in liquid nitrogen and stored at -80°C. The yield of native copurified augmin and γ-TuRC from HAUS8-GFP-Strep knock-in cells was ~0.5 and ~0.09 μg per 15-cm dish, respectively. The yield of native copurified augmin and γ-TuRC from HAUS8-GFP-Strep/GCP2-SNAP double knock-in cells was ~0.2 and ~0.03 μg per 15-cm dish, respectively.

Purification of recombinant augmin complex

For recombinant augmin complex used in Fig. 3, A and G, one 15-cm dish of HEK293T cells at ~70% confluence was cotransfected with 30 μg pTT5Multi-HAUS6-GFP (mCherry/SNAP)-Strep/HAUS2/HAUS8/HAUS3 and 30 μg pTT5Multi-HAUS7/HAUS5/HAUS4/HAUS1. 20 h after transfection, cells were treated with 200 ng/ml nocodazole for 16 h before harvesting. After the medium was removed, cells were collected with 10 ml cold PBS, followed by centrifugation at 1,000 rpm for 5 min. Then cell pellets were lysed in 1 ml lysis buffer (50 mM Hepes, 300 mM NaCl, 1 mM EGTA, 1 mM MgCl₂, 0.5% Triton X-100, and 1 mM DTT, pH 7.4) containing EDTA-free protease inhibitors (Roche) for 10 min on ice. The cell lysate was centrifuged at 14,000 rpm, 4°C for 20 min, and the supernatant was incubated with 60 μl StrepTactin beads at 4°C for 45 min. After removing the supernatant by centrifuging at 3,000 rpm and 4°C for 1 min, beads were washed four times with 1 ml lysis buffer and twice with 1 ml wash buffer B (50 mM Hepes, 150 mM NaCl, 1 mM EGTA, 1 mM MgCl₂, 0.01% Triton X-100, and 1 mM DTT, pH 7.4) by inverting the tube four to six times. Subsequently, in the case of GFP/mCherry-Strep-tagged augmin, proteins were eluted with 60 μl elution buffer (50 mM Hepes, 150 mM NaCl, 1 mM EGTA, 1 mM MgCl₂, 0.01% Triton X-100, 1 mM DTT, and 2.5 mM

desthiobiotin, pH 7.4), while in the case of SNAP-Strep-tagged augmin, to label the SNAP-tagged HAUS6, beads were incubated with 100 μl wash buffer B containing 10 μM SNAP-Surface Alexa Fluor 647 (NEB) at 4°C for 1 h in darkness, followed by washing four times with 1 ml lysis buffer and twice with 1 ml wash buffer C (50 mM Hepes, 300 mM NaCl, 1 mM EGTA, 1 mM MgCl₂, 0.01% Triton X-100, 1 mM DTT, pH 7.4) by inverting the tube four to six times and the final elution step using 60 μl elution buffer with 300 mM instead of 150 mM NaCl. All purified proteins were snap-frozen in liquid nitrogen and stored at -80°C. The yield of recombinant augmin was ~10 μg per 15-cm dish.

Purification of recombinant γ-TuRC

For recombinant γ-TuRC used in Fig. 3, F and G; and Fig. S3 F, one 15-cm dish of HEK293T cells at ~70% confluence were cotransfected with 20 μg pTT5Multi-GCP3-GFP-Strep/GCP2/γ-tubulin/γ-tubulin, 20 μg pTT5Multi-GCP4/GCP6/GCP5, and 10 μg pTT5Multi-MZT2A/MZT2B/MZT1/NME7/NEDD1. 20 h after transfection, cells were treated with 200 ng/ml nocodazole for 16 h before harvesting. After removing the medium, cells were collected with 10 ml cold PBS, followed by centrifugation at 1,000 rpm for 5 min. Then cell pellets were lysed in 1 ml lysis buffer (50 mM Hepes, 150 mM NaCl, 1 mM EGTA, 1 mM MgCl₂, 0.5% Triton X-100, 0.1 mM GTP, and 1 mM DTT, pH 7.4) containing EDTA-free protease inhibitors (Roche) for 10 min on ice. The cell lysate was centrifuged at 14,000 rpm, 4°C for 20 min, and the supernatant was incubated with 50 μl StrepTactin beads (GE Healthcare) at 4°C for 45 min. After removing the supernatant by centrifuging at 3,000 rpm, 4°C for 1 min, beads were washed four times with 1 ml lysis buffer and twice with 1 ml wash buffer A (50 mM Hepes, 150 mM NaCl, 1 mM EGTA, 1 mM MgCl₂, 0.01% Triton X-100, 0.1 mM GTP, and 1 mM DTT, pH 7.4) by inverting the tube four to six times. Finally, proteins were eluted with 60 μl elution buffer (50 mM Hepes, 150 mM NaCl, 1 mM EGTA, 1 mM MgCl₂, 0.01% Triton X-100, 0.1 mM GTP, 1 mM DTT, and 2.5 mM desthiobiotin, pH 7.4), snap-frozen and stored at -80°C. The yield of recombinant γ-TuRC was ~15 μg per 15-cm dish.

Copurification of recombinant augmin-γ-TuRC complex

For recombinant augmin-γ-TuRC complex used in Figs. 3 H and S3 L, one 15-cm dish of HEK293T cells at ~70% confluence were cotransfected with 20 μg pTT5Multi-HAUS6-mCherry-Strep/HAUS2/HAUS8/HAUS3, 20 μg pTT5Multi-HAUS7/HAUS5/HAUS4/HAUS1, 10 μg pTT5Multi-GCP3-GFP/GCP2/γ-tubulin/γ-tubulin, 10 μg pTT5Multi-GCP4/GCP6/GCP5, and 5 μg pTT5Multi-MZT2A/MZT2B/MZT1/NME7/NEDD1. The subsequent steps were the same as described in the “purification of recombinant γ-TuRC” section. The yield of recombinant copurified augmin and γ-TuRC was ~3 and ~1.2 μg per 15-cm dish, respectively.

Purification of recombinant augmin, γ-TuRC, and augmin-γ-TuRC complex in the presence of kinases or inhibitors

For recombinant augmin^{CDK1/PLK1} complex used in Figs. 6, 7, 8, and 9; and Figs. S4 and S5, one 15-cm dish of HEK293T cells at

~70% confluence was co-transfected with 20 μg pTT5Multi-HAUS6-GFP (mCherry/SNAP)-Strep/HAUS2/HAUS8/HAUS3, 20 μg pTT5Multi-HAUS7/HAUS5/HAUS4/HAUS1, 5 μg pTT5-3*HA-PLK1, and 5 μg pTT5Multi-cyclin B/CDK1. The subsequent steps were almost identical as described in the “purification of recombinant augmin complex” section, except that 0.1 mM ATP was included in the lysis buffer.

For recombinant augmin^{RO/BI} complex used in Figs. 6, 7, 8, and 9; and Figs. S4 and S5, one 15-cm dish of HEK293T cells at ~70% confluence was co-transfected with 20 μg pTT5Multi-HAUS6-GFP/mCherry/SNAP-Strep/HAUS2/HAUS8/HAUS3 and 20 μg pTT5Multi-HAUS7/HAUS5/HAUS4/HAUS1. 20 h after transfection, cells were treated simultaneously with 200 ng/ml nocodazole and 300 nM BI2536 for 16 h before harvesting. 5 μM RO3306 was also added to the media for the last 6 h of incubation with the drugs. The subsequent steps were the same as described in the “purification of recombinant augmin complex” section.

The yield of recombinant augmin^{CDK1/PLK1} and augmin^{RO/BI} was ~10 μg per 15-cm dish.

For recombinant γ -TuRC^{SIN/CDK1/PLK1} and γ -TuRC^{AWD/SIN/CDK1/PLK1} used in Figs. 6, 7, 8, S4, and S5, one (Fig. 6, 7, and S4) or three (Figs. 8 and S5) 15-cm dishes were used. One 15-cm dish of HEK293T cells at ~70% confluence was cotransfected with 20 μg pTT5Multi-GCP3-GFP/GCP2/ γ -tubulin/ γ -tubulin, 20 μg pTT5Multi-GCP4/GCP6/GCP5, 10 μg pTT5Multi-MZT2A/MZT2B/MZT1/NME7, 5 μg pTT5-3*HA-PLK1, 5 μg pTT5Multi-cyclin B/CDK1 together with 5 μg pTT5-Strep-NEDD1 or pTT5-Strep-NEDD1 Δ WD. The subsequent steps were almost identical as described in the “purification of recombinant γ -TuRC” section, except that 0.1 mM ATP was included in the lysis buffer. The yield of γ -TuRC^{SIN/CDK1/PLK1} and γ -TuRC^{AWD/SIN/CDK1/PLK1} was ~15 and ~25 μg per 15-cm dish, respectively. The yield of Strep-NEDD1 and Strep-NEDD1 Δ WD was ~7 and ~4 μg per 15-cm dish, respectively.

For recombinant γ -TuRC^{SIN/RO/BI} used in Figs. 6 and S4, one 15-cm dish of HEK293T cells at ~70% confluence were co-transfected with 20 μg pTT5Multi-GCP3-GFP/GCP2/ γ -tubulin/ γ -tubulin, 20 μg pTT5Multi-GCP4/GCP6/GCP5, 10 μg pTT5Multi-MZT2A/MZT2B/MZT1/NME7, and 5 μg pTT5-Strep-NEDD1. 20 h after transfection, cells were treated simultaneously with 200 ng/ml nocodazole and 300 nM BI2536 for 16 h before harvesting. 5 μM RO3306 was also added to the media for the last 6 h of incubation with the drugs. The subsequent steps were the same as described in the “purification of recombinant γ -TuRC” section. The yield of γ -TuRC^{SIN/RO/BI} was ~15 μg per 15-cm dish.

For recombinant γ -TuRC^{G3St/CDK1/PLK1} and γ -TuRC ^{Δ N/G3St/CDK1/PLK1} used in Fig. 7, A and D, one 15-cm dish of HEK293T cells at ~70% confluence was cotransfected with 20 μg pTT5Multi-GCP3-GFP-Strep/GCP2/ γ -tubulin/ γ -tubulin, 20 μg pTT5Multi-GCP4/GCP6/GCP5, 5 μg pTT5-3*HA-PLK1, 5 μg pTT5Multi-cyclin B/CDK1 together with 10 μg pTT5Multi-MZT2A/MZT2B/MZT1/NME7/NEDD1 (γ -TuRC^{G3St/CDK1/PLK1}) or pTT5Multi-MZT2A/MZT2B/MZT1/NME7 (γ -TuRC ^{Δ N/G3St/CDK1/PLK1}). The subsequent steps were almost identical as described in “Purification of recombinant γ -TuRC,” except that 0.1 mM ATP was included in the lysis

buffer. The yield of γ -TuRC^{G3St/CDK1/PLK1} and γ -TuRC ^{Δ N/G3St/CDK1/PLK1} was ~15 μg per 15-cm dish.

For recombinant augmin- γ -TuRC^{PLK1}, augmin- γ -TuRC^{CDK1}, and augmin- γ -TuRC^{CDK1/PLK1} used in Fig. 4 E, one 15-cm dish of HEK293T cells at ~70% confluence were cotransfected with 20 μg pTT5Multi-HAUS6-mCherry-Strep/HAUS2/HAUS8/HAUS3, 20 μg pTT5Multi-HAUS7/HAUS5/HAUS4/HAUS1, 10 μg pTT5Multi-GCP3-GFP/GCP2/ γ -tubulin/ γ -tubulin, 10 μg pTT5Multi-GCP4/GCP6/GCP5, 5 μg pTT5Multi-MZT2A/MZT2B/MZT1/NME7/NEDD1, together with 5 μg pTT5-3*HA-PLK1, or 5 μg pTT5Multi-cyclin B/CDK1, or combined kinases (5 μg each). The subsequent steps were almost identical as described in the “purification of recombinant γ -TuRC” section, except that 0.1 mM ATP was included in the lysis buffer. The yield of recombinant copurified augmin and γ -TuRC in the presence of kinases was ~3 and ~1.5 μg per 15-cm dish, respectively.

Purification of recombinant NEDD1

For recombinant NEDD1^{CDK1/PLK1} proteins used in Fig. 7, C and D, one 15-cm dish of HEK293T cells were co-transfected with 40 μg pTT5-Strep-NEDD1, 10 μg pTT5-3*HA-PLK1, and 10 μg pTT5Multi-cyclin B/CDK1. The subsequent steps were almost the same as described in Purification of recombinant augmin complex, except that 0.1 mM ATP was included in the lysis buffer.

For recombinant NEDD1 proteins used in Fig. 8, A and C, one 15-cm dish of HEK293T cells at ~70% confluence were transfected with 40 μg pTT5-NEDD1-GFP-Strep or its deletion mutants. The subsequent steps were the same as described in the “purification of recombinant augmin complex” section.

For recombinant NEDD1-GFP^{CDK1/PLK1} used in Fig. 9, B and C; and Fig. S5 E, one 15-cm dish of HEK293T cells at ~70% confluence were co-transfected with 40 μg pTT5-NEDD1-GFP-Strep, 10 μg pTT5-3*HA-PLK1, and 10 μg pTT5Multi-cyclin B/CDK1. The subsequent steps were almost identical as described in the “purification of recombinant augmin complex” section, except that 0.1 mM ATP was included in the lysis buffer.

For recombinant NEDD1-GFP^{RO/BI} used in Fig. 9, B and C; and Fig. S5 E, one 15-cm dish of HEK293T cells at ~70% confluence were transfected with 40 μg pTT5-NEDD1-GFP-Strep. 20 h after transfection, cells were treated simultaneously with 200 ng/ml nocodazole and 300 nM BI2536 for 16 h before harvesting. 5 μM RO3306 was also added to the media for the last 6 h of incubation with the drugs. The subsequent steps were the same as described in the “purification of recombinant augmin complex” section.

The yield of recombinant NEDD1 and its deletion mutants was ~10–15 μg per 15-cm dish.

Purification of recombinant augmin and NEDD1 for pull-down assay

For recombinant augmin^{CDK1} or augmin^{PLK1} complex shown in Fig. 6, D and E, one 15-cm dish of HEK293T cells at ~70% confluence was cotransfected with 20 μg pTT5Multi-HAUS6-GFP-Strep/HAUS2/HAUS8/HAUS3 and 20 μg pTT5Multi-HAUS7/HAUS5/HAUS4/HAUS1 together with 5 μg pTT5Multi-cyclin B/CDK1 or 5 μg pTT5-3*HA-PLK1. The subsequent steps were almost identical as described in Purification of recombinant augmin complex, except that 0.1 mM ATP was included in the

lysis buffer and that the augmin proteins were finally immobilized on StrepTactin beads, with the elution step being omitted.

For recombinant augmin^{RO} or augmin^{BI} complex shown in Fig. 6, D and E, one 15-cm dish of HEK293T cells at ~70% confluence was cotransfected with 20 µg pTT5Multi-HAUS6-GFP-Strep/HAUS2/HAUS8/HAUS3 and 20 µg pTT5Multi-HAUS7/HAUS5/HAUS4/HAUS1. 20 h after transfection, in the case of augmin^{RO}, cells were treated with 200 ng/ml nocodazole before harvesting, and 5 µM RO3306 was added to the medium for the last 6 h of incubation; in the case of augmin^{BI}, cells were treated simultaneously with 200 ng/ml nocodazole and 300 nM BI2536 for 16 h before harvesting. The subsequent steps were almost identical as described in the “purification of recombinant augmin complex” section, except that the augmin proteins were finally immobilized on StrepTactin beads, with the elution step being omitted.

For recombinant NEDD1^{CDK1} or NEDD1^{PLK1} shown in Fig. 6, D and E, one 15-cm dish of HEK293T cells at ~70% confluence were co-transfected with 40 µg pTT5-3*Flag-NEDD1 together with 10 µg pTT5Multi-cyclin B/CDK1 or 10 µg pTT5-3*HA-PLK1. 20 h post-transfection, cells were treated with 200 ng/ml nocodazole for 16 h before harvesting. After removing the medium, cells were collected with 10 ml cold PBS, followed by centrifugation at 1,000 rpm for 5 min. Then cell pellets were lysed in 1 ml lysis buffer (50 mM Hepes, 300 mM NaCl, 1 mM EGTA, 1 mM MgCl₂, 0.5% Triton X-100, 0.1 mM ATP, and 1 mM DTT, pH 7.4) containing EDTA-free protease inhibitors (Roche) for 10 min on ice. The cell lysate was centrifuged at 14,000 rpm, 4°C for 20 min, and the supernatant was incubated with 40 µl Anti-DYKDDDDK Affinity Beads (SA042001; SMART) at 4°C for 45 min. After the supernatant was removed by centrifuging at 3,000 rpm, 4°C for 1 min, beads were washed four times with 1 ml lysis buffer and twice with 1 ml wash buffer B (50 mM Hepes, 150 mM NaCl, 1 mM EGTA, 1 mM MgCl₂, 0.01% Triton X-100, and 1 mM DTT, pH 7.4) by inverting the tube four to six times. Finally, proteins were eluted with 100 µl elution buffer (50 mM Hepes, 150 mM NaCl, 1 mM MgCl₂, 1 mM EGTA, 0.01% Triton X-100, 1 mM DTT, and 100 ng/ml 3*Flag Peptide, pH 7.4), snap-frozen, and stored at -80°C.

For recombinant NEDD1^{RO} or NEDD1^{BI} shown in Fig. 6, D and E, one 15-cm dish of HEK293T cells at ~70% confluence was transfected with 40 µg pTT5-3*Flag-NEDD1. 20 h after transfection, in the case of NEDD1^{RO}, cells were treated with 200 ng/ml nocodazole before harvesting, and 5 µM RO3306 was also added to the media for the last 6 h of incubation with the drugs; while in the case of NEDD1^{BI}, cells were treated simultaneously with 200 ng/ml nocodazole and 300 nM BI2536 for 16 h before harvesting. The subsequent steps were almost identical as described above for the purification of flag tagged NEDD1^{CDK1} or NEDD1^{PLK1}, except that 0.1 mM ATP was omitted in the lysis buffer.

The concentration of purified proteins was determined from gel band intensities using protein molecular weight marker and BSA standard as control. For protein complex, 2~3 gel bands representing different subunits were chosen to reduce measurement error. Specifically, for augmin in all preparations, gel bands of HAUS4 and HAUS7, assumed to be one copy each in

augmin complex, were chosen for measurements; for native γ-TuRC in Fig. S1 F, gel bands of γ-tubulin (14 copies in γ-TuRC), GCP2 (5 copies in γ-TuRC), and GCP3 (5 copies in γ-TuRC) were chosen for measurements; for native γ-TuRC in Fig. S2 E, gel bands of γ-tubulin and GCP3 were chosen for measurements; for recombinant γ-TuRC shown in Fig. S3, E, K, and O; Fig. S4 E; and Fig. S5 A, gel bands of γ-tubulin and GCP2 were chosen for measurements. NEDD1 concentration refers to monomer concentration. A brief overview of the tagging and purification strategies used in this study is provided in Table S2.

Determination of the labeling efficiency of SNAP–Alexa Fluor 647

Recombinant Strep-SNAP was used instead of native γ-TuRC-SNAP to determine the labeling efficiency of SNAP–Alexa Fluor 647 because the amount of γ-TuRC-SNAP in the native augmin–γ-TuRC complex was low and thus not suitable for such analysis. The purification steps and labeling steps for the recombinant Strep-SNAP were similar to those described above for the recombinant augmin-SNAP-Strep. However, as the total amount of SNAP proteins immobilized on beads was ~30 µg from one 15 cm dish, higher than augmin-SNAP, during labeling, instead of 10 µM SNAP-Surface Alexa Fluor 647 used for augmin-SNAP, 30 µM SNAP-Surface Alexa Fluor 647 were used for SNAP to achieve a SNAP dye to SNAP protein molar ratio >2:1. The labeling efficiency of SNAP–Alexa Fluor 647 was ~90% as determined using the “Proteins and Labels” application on Nanodrop 2,000.

Pull-down assays

StrepTactin pull-down assay

For StrepTactin pull-down assays in Fig. 1 A; Fig. 4, A and B; and Fig. S1 D, HAUS8 -GFP-Strep knock-in HeLa cells seeded on 10-cm dishes were treated with 200 ng/ml nocodazole for 16 h before harvesting. The condition without nocodazole treatment was included as a control in Fig. 1 A. For assays in Fig. 4, A and B, 300 nM BI2536 or 5 µM RO3306 was also added for indicated time periods before harvesting. Then cells were washed once with cold PBS and lysed in 300 µl lysis buffer (50 mM Hepes, 150 mM NaCl, 1 mM EGTA, 1 mM MgCl₂, 0.5% Triton X-100, and 1 mM DTT, pH 7.4) containing EDTA-free protease inhibitors (Roche) for 10 min on ice. The cell lysate was centrifuged at 14,000 rpm, 4°C for 15 min, and then the supernatant was incubated with 15 µl StrepTactin beads for 45 min at 4°C. The beads were washed three times with 300 µl wash buffer (50 mM Hepes, 150 mM NaCl, 1 mM EGTA, 1 mM MgCl₂, 0.1% Triton X-100, and 1 mM DTT, pH 7.4) by inverting the tube four to six times and then subjected to Western blotting with indicated antibodies.

For StrepTactin pull-down assays in Fig. 6, F and G, ~0.5 µg indicated versions of Flag-tagged NEDD1 proteins (prey) diluted in 100 µl lysis buffer (50 mM Hepes, 150 mM NaCl, 1 mM EGTA, 1 mM MgCl₂, 0.5% Triton X-100, and 1 mM DTT, pH 7.4) were incubated with ~2 µg indicated versions of augmin-GFP-Strep-bound StrepTactin beads (bait) at 4°C for 45 min. Subsequently, beads were washed three times with 300 µl wash buffer (50 mM Hepes, 150 mM NaCl, 1 mM EGTA, 1 mM MgCl₂, 0.1% Triton

X-100, and 1 mM DTT, pH 7.4) by inverting the tube four to six times, and then subjected to Western blotting with indicated antibodies.

Streptavidin pull-down assay

For Streptavidin pull-down assays (Fig. 4, C and D; Fig. 5, A–D, F, and H; Fig. 6, A and C; and Fig. S4, A and C), HEK293T cells seeded on 6-well plates were cotransfected with indicated Bio- or Bio-GFP-tagged bait construct, HA- or GFP-tagged prey construct, and BirA construct (3 µg total DNA). 20 h after transfection, cells were treated with 200 ng/ml nocodazole for 16 h before harvesting. Then cells were washed once with cold PBS and lysed in 100 µl lysis buffer (50 mM Hepes, 150 mM NaCl, 1 mM EGTA, 1 mM MgCl₂, 0.5% Triton X-100, and 1 mM DTT, pH 7.4) containing EDTA-free protease inhibitors (Roche) for 5 min on ice. The cell lysate was centrifuged at 14,000 rpm, 4°C for 15 min, and then the supernatant was incubated with 15 µl Streptavidin-coated magnetic beads (Dynabeads M-280; Invitrogen) for 45 min at 4°C. Subsequently, beads were washed three times with 300 µl wash buffer (50 mM Hepes, 150 mM NaCl, 1 mM EGTA, 1 mM MgCl₂, 0.1% Triton X-100, and 1 mM DTT, pH 7.4) by inverting the tube four to six times, and then subjected to Western blotting with indicated antibodies.

In vitro kinase assay

2 µg Strep-GFP-tagged NEDD1 WT or NEDD1 S411A proteins were incubated with 40 ng purified Strep-cyclin B/CDK1 in the kinase reaction buffer (50 mM Hepes, 150 mM NaCl, 1 mM EGTA, 1 mM MgCl₂, 1 mM DTT, and 50 µM ATP, pH 7.4) supplemented with 5 µCi [γ -³²P] ATP (PerkinElmer) for 30 min at 30°C. The reactions were stopped by adding SDS sample buffer and boiling and then analyzed by SDS-PAGE and autoradiography.

Immunofluorescence

Cells seeded on glass coverslips in 24-well plates were fixed with different methods. For staining of MT, γ -tubulin, or SNAP in HAUS8-GFP-Strep knock-in or HAUS8-GFP-Strep/GCP2-SNAP double knock-in HeLa cells, cells were fixed sequentially in –20°C methanol for 5 min and in PBS containing 4% formaldehyde for 5 min at RT. For staining HAUS8 or NEDD1 in HeLa cells, cells were fixed in –20°C methanol for 10 min. Next, cells were permeabilized with 0.15% Triton X-100 in PBS for 2 min and blocked with 2% BSA in PBST (PBS with 0.05% Tween-20; blocking solution) for 20 min. Then incubation with primary antibody and secondary antibody diluted in blocking solution was performed at RT for 1 h and 45 min, respectively. Each incubation step was followed by three washes (5 min each) with PBST. Finally, coverslips were rinsed with 70 and 100% ethanol, air-dried, and mounted with Vectashield mounting medium (Vector Laboratories) on glass slides. Slides were stored at –20°C.

Images were captured using Nikon Ni-U with a 60× 1.40-NA oil objective equipped with a DS-Qi2 camera (Nikon) for acquisition.

In vitro MT assays

Double-cycled GMPCPP MT seeds were made as described before (Huang et al., 2021). Briefly, 14 µM unlabeled porcine brain tubulin (Cytoskeleton), 2.4 µM rhodamine-tubulin or Fluorescent HiLyte 647 tubulin (Cytoskeleton), 3.6 µM biotin-tubulin

(Cytoskeleton), and 1 mM GMPCPP (Jena Biosciences) were mixed in MRB80 buffer (80 mM PIPES, 1 mM EGTA, and 4 mM MgCl₂, pH 6.8) to a final volume of 8 µl. The tubulin reaction mixture was first placed on ice for 5 min and then incubated at 37°C for 30 min in darkness. Subsequently, MTs were pelleted by centrifugation in an Airfuge (Beckman) at ~28 psi (90,000 rpm, 160,000 g) for 5 min. After removing the supernatant carefully, the pellet was resuspended in 6 µl MRB80 buffer and depolymerized for 20 min on ice. The second round of polymerization was then performed with freshly supplemented 1 mM GMPCPP at 37°C for 30 min. Subsequently, the MT seeds were pelleted as described above and resuspended in 60 µl MRB80 buffer containing 10% glycerol, snap-frozen in 2 µl aliquots, and stored in a –80°C freezer.

In vitro assays with dynamic MTs were performed following the previously described procedure (Jiang et al., 2017). The assay flow chamber, prepared by sticking plasma-cleaned glass coverslips onto microscope slides, was incubated first with 0.2 mg/ml PLL-PEG-biotin (Susos AG) and then with 1 mg/ml neutravidin (Invitrogen) in MRB80 buffer. Subsequently, GMPCPP MT seeds were attached to the functionalized coverslip through biotin–neutravidin interactions. The flow chamber was further blocked with 1 mg/ml κ -casein. The reaction mixture, which consisted of purified proteins and MRB80 buffer containing 20 µM porcine brain tubulin, 0.5 µM rhodamine-tubulin, or Fluorescent HiLyte 647 tubulin, 1 mM GTP, 0.2 mg/ml κ -casein, 0.1% methylcellulose, and oxygen scavenger mix (50 mM glucose, 400 µg/ml glucose oxidase, 200 µg/ml catalase, and 4 mM DTT) was added to the chamber after centrifugation in an Airfuge for 5 min at ~28 psi (90,000 rpm, 160,000 g). The flow chamber was sealed with vacuum grease, and the sample was imaged immediately at 30°C with a total internal reflection fluorescence (TIRF) microscope. The imaging interval was 2 s unless stated otherwise.

For assays in the presence of recombinant γ -TuRC or native and recombinant augmin- γ -TuRC complex, these proteins were separately centrifuged at 14,000 rpm (18,000 g), 4°C for 5 min, because ultra-high-speed centrifugation in an Airfuge could result in ~40% loss of γ -TuRC. The clarified supernatant was then added into the reaction mixture excluding these proteins prepared by the abovementioned ultra-high-speed centrifugation.

For assays in the presence of augmin-mCherry or γ -TuRC-GFP-augmin-mCherry complex, HiLyte 647-labeled GMPCPP seeds and HiLyte 647 tubulin were used instead of rhodamine-labeled GMPCPP seeds and rhodamine-tubulin.

For assays to determine the MT nucleation activity of recombinant γ -TuRC, γ -TuRC^{S₅N/CDK1/PLK1}, and γ -TuRC ^{Δ WD/S₅N/CDK1/PLK1} at indicated concentrations (Figs. S3 F and S5 B), incubation with neutravidin and GMPCPP seeds steps were omitted.

TIRF microscopy

TIRF microscopy was performed on Nikon Eclipse Ti2-E (Nikon) with the perfect focus with the Nikon CFI Apo TIRF 100× 1.49 N.A. oil objective (Nikon), Prime 95B camera (Photometrics), SOLE laser engine (four lasers: 405, 488, 561, and 638 nm; Omicron) and controlled by NIS-Elements software (Nikon). Images were magnified with a 1.5× intermediate lens on Ti2-E

before being projected onto the camera. The resulting pixel size is 73.3 nm/pixel. Stage-top incubator INUBG2E-ZILCS (Tokai Hit) was used to keep *in vitro* samples at 30°C. All adjustable imaging parameters (TIRF angle, laser intensity, and exposure time) were kept the same within experiments.

For branching MT nucleation assays with native complexes *in vitro*, images were collected for 25 min with an interval of 4 s. For branching MT nucleation assays with recombinant complexes *in vitro*, the images were collected for 15 min with an interval of 4 s. For other *in vitro* MT assays, the images were collected for 10 min with an interval of 2 s.

Optosplit III beamsplitter (Cairn Research) was used for simultaneous imaging of red and green fluorescence. The sequential acquisition was used for three- or four-color imaging experiments.

Image processing

For measurement of branching/landing ratio (Fig. S2, J and K), a circular region of interest (ROI) was selected to cover the augmin-GFP and γ -TuRC-SNAP/AF647 double-positive puncta that initiate the branching nucleation. The “landing” intensity was defined as the intensity of augmin-GFP or γ -TuRC-SNAP/AF647 averaged from three consecutive frames (time interval of 4 s), with the first frame being the exact time point of the complex landing. Similarly, the “branching” intensity was defined as the intensity of augmin-GFP or γ -TuRC-SNAP/AF647 averaged from three consecutive frames, with the first frame being the exact time point of branching nucleation. The branching intensity was divided by the landing intensity to calculate the branching/landing ratio. For plots of augmin intensity (green) and γ -TuRC intensity (blue) of the branching nucleation-competent puncta against time (Fig. S2 L), the puncta were tracked, and their intensities were measured using an ImageJ macro, QuickPALM.

The distribution of branching sites along the length of newly generated GDP-MTs (Figs. 1 H and S2 F) was measured using the line tool in ImageJ by drawing a line from the branching site to the plus end or minus end of the GMPCPP seed (distance 1 [+] or distance 1 [-]) for the primary branching events, or from the daughter branching site and the mother branching site (termed distance 2) for the secondary and tertiary branching events. Distance 1 (+), or distance 1 (-), or distance 2 was then divided by the total length of the mother MT at the time of branching to calculate the corresponding fractional distance.

For measurement of the intensity of HAUS8 and NEDD1 along the spindle (Fig. S4, I, J, M, and N), a trapezoid ROI was selected to cover the spindle. For measurement of the intensity of NEDD1 at the centrosome (Fig. S4, J and N), a circular ROI was selected to cover the centrosome structure.

Plots were generated using Excel (Microsoft) or Prism (GraphPad) software. Images were prepared for publication using ImageJ and Adobe Photoshop.

Single-molecule counting assay

To determine the oligomeric state of augmin in solution, we added diluted samples of purified GFP, EB3-GFP, and native augmin-GFP/ γ -TuRC-SNAP/AF647 co-complex to the parallel flow chambers made on the same plasma cleaned coverslip. Similarly, to determine the oligomeric state of γ -TuRC, we used

SNAP/AF647, EB3-SNAP/AF647, and native augmin-GFP/ γ -TuRC-SNAP/AF647 co-complex. After washing with MRB80, GFP or SNAP/AF647-fused molecules immobilized on the coverslip were imaged at 30°C by TIRF microscopy. Each diluted sample contained 1,000–2,000 individual spots per field of view ($88 \times 88 \mu\text{m}$), and the central area ($40 \times 40 \mu\text{m}$) was selected for measurements. A set of 40 images per condition with 500-ms exposure for the GFP channel and 1-s exposure for the Alexa Fluor 647 channel was acquired blindly at diverse places of the coverslip to avoid prebleaching. Single-molecule fluorescent spots were detected, and their intensities were measured using QuickPALM. Histograms of fluorescence intensity were built using Excel. Histograms were fitted to Gaussian distribution using Origin software to determine the mean intensity of GFP- or SNAP/AF647-fused single molecules.

To estimate the number of augmin and γ -TuRC molecules at the branching sites, we immobilized single molecules of GFP or SNAP/AF647 in one of the flow chambers on the coverslip and performed an *in vitro* MT dynamics assay using native augmin-GFP/ γ -TuRC-SNAP co-complex in the neighboring chamber of the same coverslip. Using the same illumination parameters (100-ms exposure for the GFP channel and 300-ms exposure for the Alexa Fluor 647 channel), we collected images of unbleached single molecules of GFP or SNAP/AF647 and performed time-lapse imaging of the *in vitro* MT dynamics assay with native augmin-GFP/ γ -TuRC-SNAP co-complex. The fitted mean intensity of GFP or SNAP/AF647 was obtained as described above. QuickPALM was used to measure the intensity of augmin-GFP and γ -TuRC-SNAP/AF647 double-positive puncta that initiate the branching nucleation. The landing intensity was defined as the intensity of augmin-GFP or γ -TuRC-SNAP/AF647 averaged from three consecutive frames (time interval of 4 s), with the first frame being the exact time point of the complex landing. Similarly, the branching intensity was defined as the intensity of augmin-GFP or γ -TuRC-SNAP/AF647 averaged from three consecutive frames, with the first frame being the exact time point of branching nucleation. The number of augmin-GFP or γ -TuRC-SNAP molecules was calculated by dividing the intensity of augmin-GFP or γ -TuRC-SNAP at branch sites by the fitted mean intensity of GFP or SNAP, respectively.

Mass spectrometry

To identify augmin-binding proteins, the endogenous HAUS8-GFP-Strep and its binding partners were pulled down using StrepTactin beads from HeLa HAUS8-GFP-Strep knock-in cells, which were arrested in mitosis by 200 ng/ml nocodazole treatment for 16 h. To determine the purity of the recombinant augmin-GFP, recombinant γ -TuRC-GFP, and recombinant augmin-mCherry- γ -TuRC-GFP complex purified from HEK293T cells, $\sim 5\text{--}10 \mu\text{g}$ proteins were used for mass spectrometry analysis. The samples were run on SDS-PAGE gel for 1 cm. After staining the gel with Coomassie dye G-250, the lane was cut and subjected to mass spectrometry using a UHR-QqTOF mass spectrometer (Bruker) and PEAKS 8.5 software (BSI).

Statistical analysis

Statistical analysis was performed with Excel (Microsoft). P values were determined by unpaired two-tailed *t* test. ***, $P < 0.001$. Data distribution was assumed to be normal but was not formally tested.

Online supplemental material

Fig. S1 characterizes HAUS8-GFP-Strep knock-in HeLa cell lines. **Fig. S2** characterizes HAUS8-GFP-Strep/GCP2-SNAP double knock-in HeLa cell lines. **Fig. S3** shows the construction of pTT5Multi vector-based plasmids for coexpression of the 8 components of augmin and 11 components of γ -TuRC. **Fig. S4** shows that PLK1- and CDK1-dependent phosphorylation is essential for branching MT nucleation in vitro and important for the spindle localization of augmin and γ -TuRC in cells. **Fig. S5** characterizes the contribution of NEDD1 WD to γ -TuRC's nucleation activity and the synergistic MT-binding activities between NEDD1 and augmin. **Video 1** shows the reconstitution of branching MT nucleation using purified native augmin- γ -TuRC complex. **Video 2** shows the closer inspection of branching events that occurred from a single GMPCPP seed. **Videos 3** and **4** show the direct observation of augmin and γ -TuRC during the process of branching nucleation. **Video 5** shows the MT nucleation at different γ -TuRC concentrations. **Videos 6** and **7** show the reconstitution of branching MT nucleation using recombinant complete augmin- γ -TuRC complex. **Video 8** shows the reconstitution of more robust branching MT nucleation using recombinant complete augmin- γ -TuRC complex phosphorylated by CDK1 and PLK1. **Video 9** shows that both augmin phosphorylation and γ -TuRC phosphorylation by CDK1 and PLK1 are required for robust branching MT nucleation. **Video 10** shows that NEDD1 WD40 domain is essential for branching nucleation. Table S1 shows the analysis of native augmin- γ -TuRC complex, recombinant augmin complex, recombinant γ -TuRC, and recombinant augmin- γ -TuRC complex used for in vitro assay by mass spectrometry. Table S2 provides a brief overview of the tagging and purification strategies used in this study.

Acknowledgments

This study was supported by grants from National Natural Science Foundation of China (31871356, 32070705) and the Fundamental Research Funds for the Central Universities.

The authors declare no competing financial interests.

Author contributions: Conceptualization, K. Jiang, Y. Zhang; Investigation, Y. Zhang; Methodology, K. Jiang, S. Hua, Y. Zhang; Resources, X. Hong; Visualization, Y. Zhang, S. Hua, K. Jiang; Writing—Original Draft, K. Jiang, S. Hua, Y. Zhang; Writing—Review and Editing, K. Jiang, S. Hua; Funding Acquisition, K. Jiang; and Supervision, K. Jiang.

Submitted: 15 September 2021

Revised: 7 March 2022

Accepted: 2 May 2022

References

Alfaro-Aco, R., A. Thawani, and S. Petry. 2020. Biochemical reconstitution of branching microtubule nucleation. *Elife*. 9:e49797. <https://doi.org/10.7554/eLife.49797>

Chen, J.W.C., Z.A. Chen, K.B. Rogala, J. Metz, C.M. Deane, J. Rappsilber, and J.G. Wakefield. 2017. Cross-linking mass spectrometry identifies new interfaces of Augmin required to localise the gamma-tubulin ring complex to the mitotic spindle. *Biol. Open*. 6:654–663. <https://doi.org/10.1242/bio.022905>

Choi, Y.K., P. Liu, S.K. Sze, C. Dai, and R.Z. Qi. 2010. CDK5RAP2 stimulates microtubule nucleation by the gamma-tubulin ring complex. *J. Cell Biol.* 191:1089–1095. <https://doi.org/10.1083/jcb.201007030>

Consolati, T., J. Locke, J. Roostalu, Z.A. Chen, J. Gannon, J. Asthana, W.M. Lim, F. Martino, M.A. Cvetkovic, J. Rappsilber, et al. 2020. Microtubule nucleation properties of single human γ TuRCs explained by their cryo-EM structure. *Dev. Cell*. 53:603–617.e8. <https://doi.org/10.1016/j.devcel.2020.04.019>

Cota, R.R., N. Teixido-Travesa, A. Ezquerro, S. Eibes, C. Lacasa, J. Roig, and J. Luders. 2017. MZT1 regulates microtubule nucleation by linking γ TuRC assembly to adapter-mediated targeting and activation. *J. Cell Sci.* 130: 406–419. <https://doi.org/10.1242/jcs.195321>

Cunha-Ferreira, I., A. Chazeau, R.R. Buijs, R. Stucchi, L. Will, X. Pan, Y. Adolfs, C. van der Meer, J.C. Wolthuis, O.I. Kahn, et al. 2018. The HAUS complex is a key regulator of non-centrosomal microtubule organization during neuronal development. *Cell Rep.* 24:791–800. <https://doi.org/10.1016/j.celrep.2018.06.093>

David, A.F., P. Roudot, W.R. Legant, E. Betzig, G. Danuser, and D.W. Gerlich. 2019. Augmin accumulation on long-lived microtubules drives amplification and kinetochore-directed growth. *J. Cell Biol.* 218:2150–2168. <https://doi.org/10.1083/jcb.201805044>

Durocher, Y., S. Perret, and A. Kamen. 2002. High-level and high-throughput recombinant protein production by transient transfection of suspension-growing human 293-EBNA1 cells. *Nucleic Acids Res.* 30:E9. <https://doi.org/10.1093/nar/30.2.e9>

Goshima, G., and A. Kimura. 2010. New look inside the spindle: Microtubule-dependent microtubule generation within the spindle. *Curr. Opin. Cell Biol.* 22:44–49. <https://doi.org/10.1016/j.ccb.2009.11.012>

Goshima, G., M. Mayer, N. Zhang, N. Stuurman, and R.D. Vale. 2008. Augmin: A protein complex required for centrosome-independent microtubule generation within the spindle. *J. Cell Biol.* 181:421–429. <https://doi.org/10.1083/jcb.200711053>

Goshima, G., R. Wollman, S.S. Goodwin, N. Zhang, J.M. Scholey, R.D. Vale, and N. Stuurman. 2007. Genes required for mitotic spindle assembly in *Drosophila* S2 cells. *Science*. 316:417–421. <https://doi.org/10.1126/science.1141314>

Haren, L., M.H. Remy, I. Bazin, I. Callebaut, M. Wright, and A. Merdes. 2006. NEDD1-dependent recruitment of the gamma-tubulin ring complex to the centrosome is necessary for centriole duplication and spindle assembly. *J. Cell Biol.* 172:505–515. <https://doi.org/10.1083/jcb.200510028>

Haren, L., T. Stearns, and J. Luders. 2009. Plk1-dependent recruitment of gamma-tubulin complexes to mitotic centrosomes involves multiple PCM components. *PLoS One*. 4:e5976. <https://doi.org/10.1371/journal.pone.0005976>

Ho, C.-M.K., T. Hotta, Z. Kong, C.J.T. Zeng, J. Sun, Y.-R.J. Lee, and B. Liu. 2011. Augmin plays a critical role in organizing the spindle and phragmoplast microtubule arrays in *Arabidopsis*. *Plant Cell*. 23:2606–2618. <https://doi.org/10.1105/tpc.111.086892>

Hsia, K.C., E.M. Wilson-Kubalek, A. Dottore, Q. Hao, K.L. Tsai, S. Forth, Y. Shimamoto, R.A. Milligan, and T.M. Kapoor. 2014. Reconstitution of the augmin complex provides insights into its architecture and function. *Nat. Cell Biol.* 16:852–863. <https://doi.org/10.1038/ncb3030>

Hua, S., and K. Jiang. 2020. Expression and purification of microtubule-associated proteins from HEK293T cells for in vitro reconstitution. *Methods Mol. Biol.* 2101:19–26. https://doi.org/10.1007/978-1-0716-0219-5_2

Huang, J., Z. Liang, C. Guan, S. Hua, and K. Jiang. 2021. WDR62 regulates spindle dynamics as an adaptor protein between TPX2/Aurora A and katanin. *J. Cell Biol.* 220:e202007167. <https://doi.org/10.1083/jcb.202007167>

Huang, T.L., H.J. Wang, Y.C. Chang, S.W. Wang, and K.C. Hsia. 2020. Promiscuous binding of microprotein Mozart1 to gamma-tubulin complex mediates specific subcellular targeting to control microtubule array formation. *Cell Rep.* 31:107836. <https://doi.org/10.1016/j.celrep.2020.107836>

Hutchins, J.R.A., Y. Toyoda, B. Hegemann, I. Poser, J.K. Hérliche, M.M. Sykora, M. Augsburg, O. Hudecz, B.A. Buschhorn, J. Bulkescher, et al. 2010. Systematic analysis of human protein complexes identifies chromosome segregation proteins. *Science*. 328:593–599. <https://doi.org/10.1126/science.1181348>

Jiang, K., L. Rezaczkova, S. Hua, Q. Liu, G. Capitani, A.F.M. Altelaar, A.J.R. Heck, R.A. Kammerer, M.O. Steinmetz, and A. Akhmanova. 2017. Microtubule minus-end regulation at spindle poles by an ASPM-katanin complex. *Nat Cell Biol.* 19:480–492. <https://doi.org/10.1038/ncb3511>

Johmura, Y., N.K. Soung, J.E. Park, L.R. Yu, M. Zhou, J.K. Bang, B.Y. Kim, T.D. Veenstra, R.L. Erikson, and K.S. Lee. 2011. Regulation of microtubule-

- based microtubule nucleation by mammalian polo-like kinase 1. *Proc. Natl. Acad. Sci. USA*. 108:11446–11451. <https://doi.org/10.1073/pnas.1106223108>
- Joukov, V., J.C. Walter, and A. De Nicolo. 2014. The Cep192-organized aurora A-Plk1 cascade is essential for centrosome cycle and bipolar spindle assembly. *Mol. Cell*. 55:578–591. <https://doi.org/10.1016/j.molcel.2014.06.016>
- Kamasaki, T., E. O'Toole, S. Kita, M. Osumi, J. Usukura, J.R. McIntosh, and G. Goshima. 2013. Augmin-dependent microtubule nucleation at microtubule walls in the spindle. *J. Cell Biol.* 202:25–33. <https://doi.org/10.1083/jcb.201304031>
- Kapoor, T.M. 2017. Metaphase spindle assembly. *Biology*. 6:E8. <https://doi.org/10.3390/biology6010008>
- Knop, M., G. Pereira, S. Geissler, K. Grein, and E. Schiebel. 1997. The spindle pole body component Spc97p interacts with the gamma-tubulin of *Saccharomyces cerevisiae* and functions in microtubule organization and spindle pole body duplication. *EMBO J.* 16:1550–1564. <https://doi.org/10.1093/emboj/16.7.1550>
- Kollman, J.M., A. Merdes, L. Mourey, and D.A. Agard. 2011. Microtubule nucleation by gamma-tubulin complexes. *Nat. Rev. Mol. Cell Biol.* 12:709–721. <https://doi.org/10.1038/nrm3209>
- Lawo, S., M. Bashkurov, M. Mullin, M.G. Ferreria, R. Kittler, B. Habermann, A. Tagliaferro, I. Poser, J.R.A. Hutchins, B. Hegemann, et al. 2009. HAUS, the 8-subunit human Augmin complex, regulates centrosome and spindle integrity. *Curr. Biol.* 19:816–826. <https://doi.org/10.1016/j.cub.2009.04.033>
- Liu, L., and C. Wiese. 2008. Xenopus NEDD1 is required for microtubule organization in Xenopus egg extracts. *J. Cell Sci.* 121:578–589. <https://doi.org/10.1242/jcs.018937>
- Liu, P., Y.K. Choi, and R.Z. Qi. 2014a. NME7 is a functional component of the gamma-tubulin ring complex. *Mol. Biol. Cell*. 25:2017–2025. <https://doi.org/10.1091/mbc.E13-06-0339>
- Liu, P., E. Zupa, A. Neuner, A. Bohler, J. Loerke, D. Flemming, T. Ruppert, T. Rudack, C. Peter, C. Spahn, et al. 2020. Insights into the assembly and activation of the microtubule nucleator gamma-TuRC. *Nature*. 578:467–471. <https://doi.org/10.1038/s41586-019-1896-6>
- Liu, T., J. Tian, G. Wang, Y. Yu, C. Wang, Y. Ma, X. Zhang, G. Xia, B. Liu, and Z. Kong. 2014b. Augmin triggers microtubule-dependent microtubule nucleation in interphase plant cells. *Curr. Biol.* 24:2708–2713. <https://doi.org/10.1016/j.cub.2014.09.053>
- Luders, J., U.K. Patel, and T. Stearns. 2006. GCP-WD is a gamma-tubulin targeting factor required for centrosomal and chromatin-mediated microtubule nucleation. *Nat. Cell Biol.* 8:137–147. <https://doi.org/10.1038/ncb1349>
- Meireles, A.M., K.H. Fisher, N. Colombie, J.G. Wakefield, and H. Ohkura. 2009. Wac: A new augmin subunit required for chromosome alignment but not for acentrosomal microtubule assembly in female meiosis. *J. Cell Biol.* 184:777–784. <https://doi.org/10.1083/jcb.200811102>
- Oegema, K., C. Wiese, O.C. Martin, R.A. Milligan, A. Iwamatsu, T.J. Mitchison, and Y. Zheng. 1999. Characterization of two related Drosophila gamma-tubulin complexes that differ in their ability to nucleate microtubules. *J. Cell Biol.* 144:721–733. <https://doi.org/10.1083/jcb.144.4.721>
- Petry, S. 2016. Mechanisms of mitotic spindle assembly. *Annu. Rev. Biochem.* 85:659–683. <https://doi.org/10.1146/annurev-biochem-060815-014528>
- Petry, S., A.C. Groen, K. Ishihara, T.J. Mitchison, and R.D. Vale. 2013. Branching microtubule nucleation in Xenopus egg extracts mediated by augmin and TPX2. *Cell*. 152:768–777. <https://doi.org/10.1016/j.cell.2012.12.044>
- Petry, S., C. Pugieux, F.J. Nedelec, and R.D. Vale. 2011. Augmin promotes meiotic spindle formation and bipolarity in Xenopus egg extracts. *Proc. Natl. Acad. Sci. USA*. 108:14473–14478. <https://doi.org/10.1073/pnas.1110412108>
- Prosser, S.L., and L. Pelletier. 2017. Mitotic spindle assembly in animal cells: A fine balancing act. *Nat. Rev. Mol. Cell Biol.* 18:187–201. <https://doi.org/10.1038/nrm.2016.162>
- Sanchez-Huertas, C., F. Freixo, R. Viais, C. Lacasa, E. Soriano, and J. Luders. 2016. Non-centrosomal nucleation mediated by augmin organizes microtubules in post-mitotic neurons and controls axonal microtubule polarity. *Nat. Commun.* 7:12187. <https://doi.org/10.1038/ncomms12187>
- Song, J.G., M.R. King, R. Zhang, R.S. Kadzik, A. Thawani, and S. Petry. 2018. Mechanism of how augmin directly targets the gamma-tubulin ring complex to microtubules. *J. Cell Biol.* 217:2417–2428. <https://doi.org/10.1083/jcb.201711090>
- Takahashi, M., A. Yamagiwa, T. Nishimura, H. Mukai, and Y. Ono. 2002. Centrosomal proteins CG-NAP and kendrin provide microtubule nucleation sites by anchoring gamma-tubulin ring complex. *Mol. Biol. Cell*. 13:3235–3245. <https://doi.org/10.1091/mbc.E02-02-0112>
- Tariq, A., L. Green, J.C.G. Jeynes, C. Soeller, and J.G. Wakefield. 2020. In vitro reconstitution of branching microtubule nucleation. *Elife*. 9:e49769. <https://doi.org/10.7554/eLife.49769>
- Teixido-Travesa, N., J. Villen, C. Lacasa, M.T. Bertran, M. Archinti, S.P. Gygi, C. Caelles, J. Roig, and J. Luders. 2010. The gammaTuRC revisited: A comparative analysis of interphase and mitotic human gammaTuRC redefines the set of core components and identifies the novel subunit GCP8. *Mol. Biol. Cell*. 21:3963–3972. <https://doi.org/10.1091/mbc.E10-05-0408>
- Thawani, A., R.S. Kadzik, and S. Petry. 2018. XMAP215 is a microtubule nucleation factor that functions synergistically with the gamma-tubulin ring complex. *Nat. Cell Biol.* 20:575–585. <https://doi.org/10.1038/s41556-018-0091-6>
- Thawani, A., H.A. Stone, J.W. Shaevitz, and S. Petry. 2019. Spatiotemporal organization of branched microtubule networks. *Elife*. 8:e43890. <https://doi.org/10.7554/eLife.43890>
- Uehara, R., and G. Goshima. 2010. Functional central spindle assembly requires de novo microtubule generation in the interchromosomal region during anaphase. *J. Cell Biol.* 191:259–267. <https://doi.org/10.1083/jcb.201004150>
- Uehara, R., T. Kamasaki, S. Hiruma, I. Poser, K. Yoda, J. Yajima, D.W. Gerlich, and G. Goshima. 2016. Augmin shapes the anaphase spindle for efficient cytokinetic furrow ingression and abscission. *Mol. Biol. Cell*. 27:812–827. <https://doi.org/10.1091/mbc.E15-02-0101>
- Uehara, R., R.S. Nozawa, A. Tomioka, S. Petry, R.D. Vale, C. Obuse, and G. Goshima. 2009. The augmin complex plays a critical role in spindle microtubule generation for mitotic progression and cytokinesis in human cells. *Proc. Natl. Acad. Sci. USA*. 106:6998–7003. <https://doi.org/10.1073/pnas.0901587106>
- Verma, V., and T.J. Maresca. 2019. Direct observation of branching MT nucleation in living animal cells. *J. Cell Biol.* 218:2829–2840. <https://doi.org/10.1083/jcb.201904114>
- Wainman, A., D.W. Buster, T. Duncan, J. Metz, A. Ma, D. Sharp, and J.G. Wakefield. 2009. A new Augmin subunit, Msd1, demonstrates the importance of mitotic spindle-templated microtubule nucleation in the absence of functioning centrosomes. *Genes Dev.* 23:1876–1881. <https://doi.org/10.1101/gad.532209>
- Watanabe, S., G. Shioi, Y. Furuta, and G. Goshima. 2016. Intra-spindle microtubule assembly regulates clustering of microtubule-organizing centers during early mouse development. *Cell Rep.* 15:54–60. <https://doi.org/10.1016/j.celrep.2016.02.087>
- Wieczorek, M., T.L. Huang, L. Urnavicius, K.C. Hsia, and T.M. Kapoor. 2020a. MZT proteins form multi-faceted structural modules in the gamma-tubulin ring complex. *Cell Rep.* 31:107791. <https://doi.org/10.1016/j.celrep.2020.107791>
- Wieczorek, M., L. Urnavicius, S.C. Ti, K.R. Molloy, B.T. Chait, and T.M. Kapoor. 2020b. Asymmetric molecular architecture of the human gamma-tubulin ring complex. *Cell*. 180:165–175.e16. <https://doi.org/10.1016/j.cell.2019.12.007>
- Zheng, Y., M.L. Wong, B. Alberts, and T. Mitchison. 1995. Nucleation of microtubule assembly by a gamma-tubulin-containing ring complex. *Nature*. 378:578–583. <https://doi.org/10.1038/378578a0>
- Zhu, H., J.A. Coppinger, C.Y. Jang, J.R. Yates 3rd, and G. Fang. 2008. FAM29A promotes microtubule amplification via recruitment of the NEDD1-gamma-tubulin complex to the mitotic spindle. *J. Cell Biol.* 183:835–848. <https://doi.org/10.1083/jcb.200807046>
- Zhu, H., K. Fang, and G. Fang. 2009. FAM29A, a target of Plk1 regulation, controls the partitioning of NEDD1 between the mitotic spindle and the centrosomes. *J. Cell Sci.* 122:2750–2759. <https://doi.org/10.1242/jcs.048223>
- Zimmermann, F., M. Serna, A. Ezquerra, R. Fernandez-Leiro, O. Llorca, and J. Luders. 2020. Assembly of the asymmetric human gamma-tubulin ring complex by RUVBL1-RUVBL2 AAA ATPase. *Sci. Adv.* 6:eabe0894. <https://doi.org/10.1126/sciadv.abe0894>
- Zupa, E., P. Liu, M. Wurtz, E. Schiebel, and S. Pfeffer. 2021. The structure of the gamma-TuRC: A 25-years-old molecular puzzle. *Curr. Opin. Struct. Biol.* 66:15–21. <https://doi.org/10.1016/j.sbi.2020.08.008>

Supplemental material

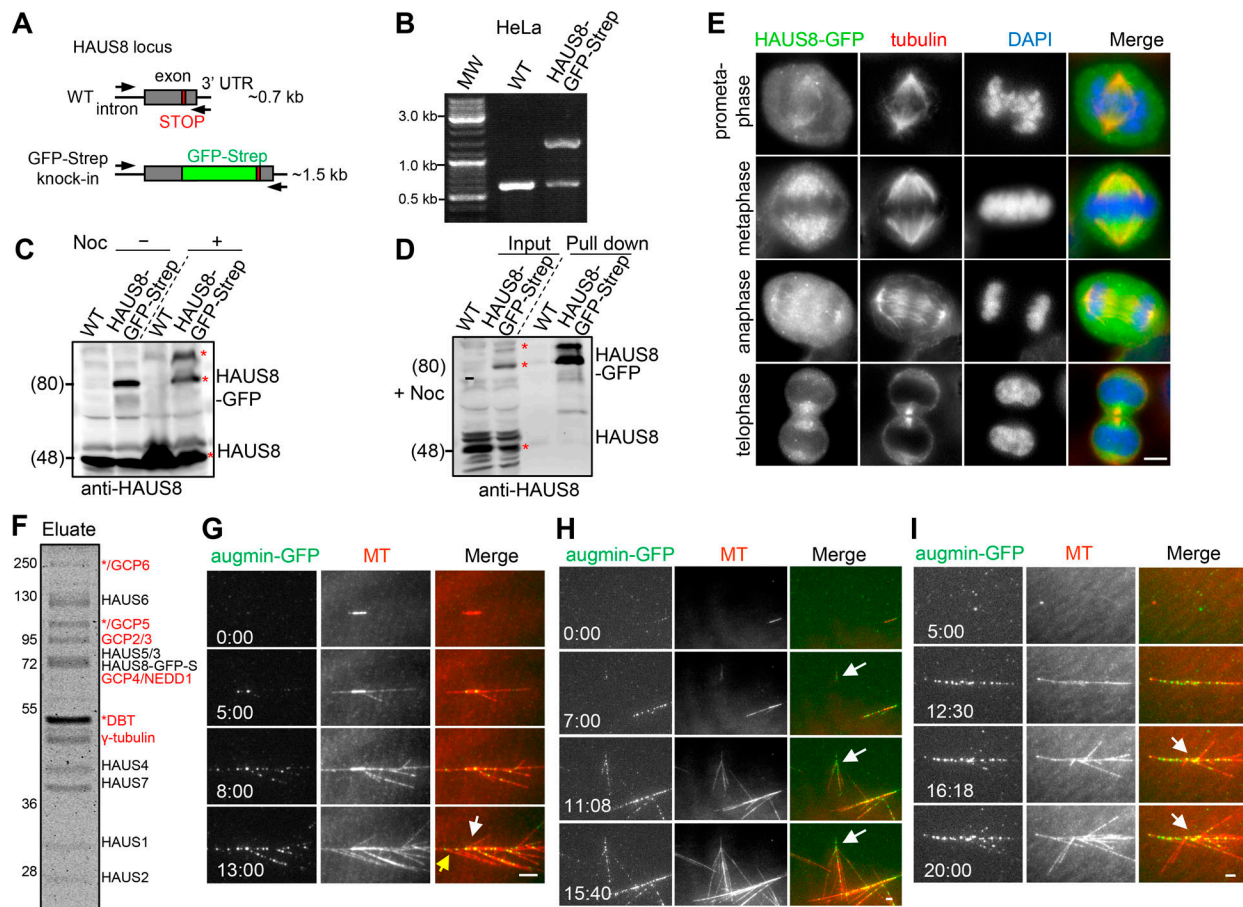


Figure S1. **Characterization of HAUS8-GFP-Strep knock-in HeLa cell lines.** (A–C) Characterization of HAUS8 knock-in HeLa cell line. (A) Schematic illustration of primer sets and the expected PCR products. PCR genotyping (B) and Western blotting analysis (C) showing that the HAUS8-GFP-Strep knock-in HeLa cell line used in this study is heterozygous. The bands corresponding to up-shifted tagged HAUS8 (nocodazole treated group), tagged, and untagged HAUS8 are marked with red asterisks in C. Of note, GFP-tagging may affect the mobility of HAUS8 on the protein gel, as band shift was only apparent for tagged but not untagged HAUS8. (D) StrepTactin pull-down assay with extracts of nocodazole-arrested mitotic control HeLa (WT) and HAUS8-GFP-Strep knock-in HeLa cells, analyzed by Western blotting with HAUS8 antibody. The bands corresponding to untagged HAUS8 (input), tagged HAUS8, and its up-shifted version (pull-down) are marked with red asterisks. (E) Immunofluorescence staining for α -tubulin and DNA (DAPI) in HAUS8-GFP-Strep knock-in HeLa cells during mitosis. (F) Coomassie blue-stained gel with native augmin- γ -TuRC complex purified from nocodazole-arrested mitotic HAUS8-GFP-Strep knock-in HeLa cells using one-step affinity purification with StrepTactin beads. S, Strep-tag. Asterisks indicate putative contaminants. Above the band of γ -tubulin, a strong band marked with an asterisk represents dihydrofolipoamide branched chain transacylase (DBT), as determined by mass spectrometry. (G) Representative images of branching MT nucleation both from GMPCPP seed (denoted by white arrow) and from GDP-MT grown from the minus end of seed (denoted by yellow arrow). (H) Representative images of de novo nucleation of branched MTs from solution (white arrows). (I) Representative images of branch formation at obtuse angles (white arrows). Scale bars, 2 μ m.

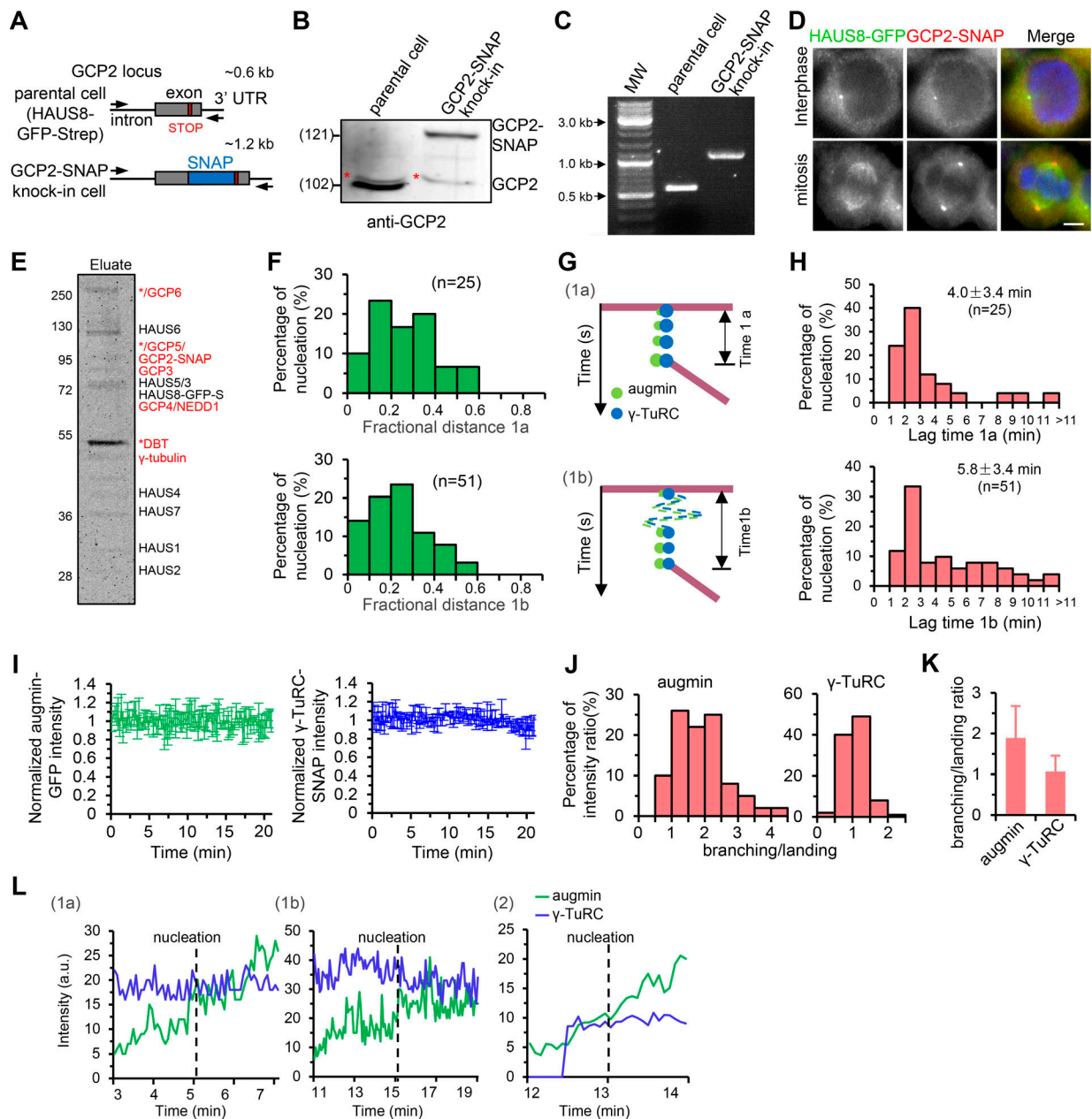


Figure S2. Characterization of HAUS8-GFP-Strep/GCP2-SNAP double knock-in HeLa cell lines. (A–C) Characterization of GCP2-SNAP knock-in based on the parental HAUS8-GFP-Strep knock-in HeLa cell line. (A) Schematic illustration of primer sets and the expected PCR products. Western blotting analysis (B) and PCR genotyping (C) showing that the GCP2-SNAP knock-in is homozygous. The red asterisk indicates a nonspecific band detected by the GCP2 antibody. (D) Immunofluorescence staining for SNAP and DNA (DAPI) in HAUS8-GFP-Strep/GCP2-SNAP double knock-in HeLa cell line. (E) Coomassie blue-stained gel with native augmin- γ -TuRC complex purified from nocodazole-arrested mitotic HAUS8-GFP-Strep/GCP2-SNAP double knock-in HeLa cells using one-step affinity purification with StrepTactin beads. Asterisks indicate putative contaminants. Above the band of γ -tubulin, a strong band marked with an asterisk represents dihydrolipoamide branched chain transacylase (DBT), as determined by mass spectrometry. (F) Distribution of fractional distance for class 1a and class 1b events. For 1a, $n = 25$; for 1b, $n = 51$. (G and H) Schematic representation (G) and histograms of distribution (H) of the lag time between the landing of augmin- γ -TuRC to the mother MT and nucleation of the daughter MT for class 1a and class 1b events. For 1a, $n = 25$; for 1b, $n = 51$. (I) Plots of intensities of single augmin-GFP (green) or γ -TuRC-SNAP/AF647 (blue) puncta attached on the surface of the coverslip rather than along the MT during the 20-min imaging window. $n = 10$ puncta from three experiments. (J) Histogram shows distribution of the ratio of augmin or γ -TuRC intensity at the time point of branching nucleation to that at the time point of the augmin- γ -TuRC complex landing (branching/landing). $n = 100$ events from 10 experiments. (K) Quantification of the average branching/landing ratio derived from J. $n = 100$ events from 10 experiments. (L) Plots of augmin intensity (green) and γ -TuRC intensity (blue) of the branching nucleation-competent puncta as indicated by red arrows in Fig. 2, F–H, against time. Scale bars, 2 μ m. Data represent mean \pm SD.

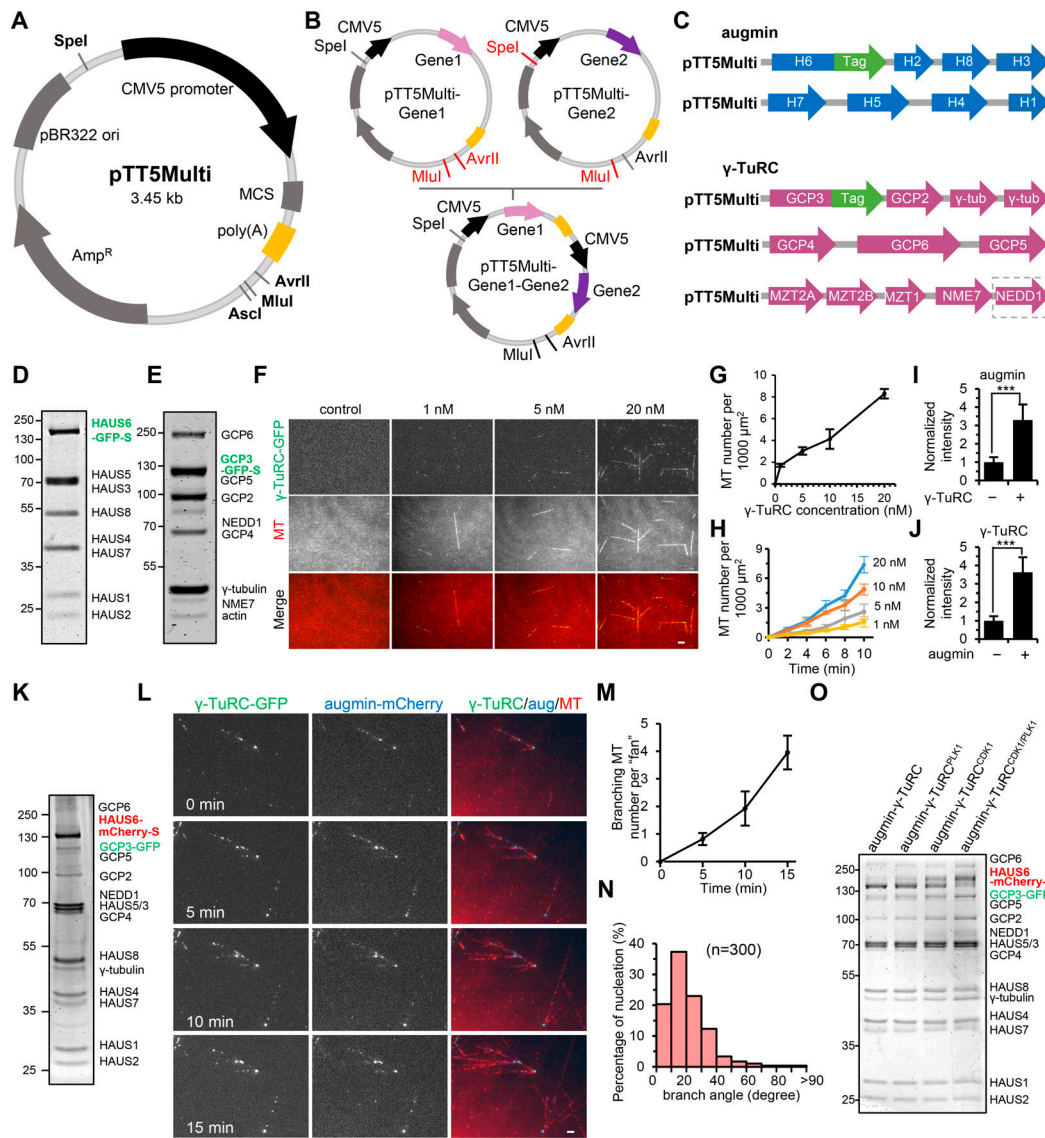


Figure S3. Construction of pTT5Multi vector-based plasmids for coexpression of the 8 components of augmin and 11 components of γ -TuRC. (A) Schematic diagram of the empty pTT5Multi vector modified from the original pTT5 vector (see Materials and methods for detailed information). Note that SpeI, AvrII, and MluI are three important restriction sites for the cloning strategy. (B) Scheme for the construction of the pTT5Multi plasmid that contains multiple gene cassettes. First, Gene1 and Gene2 were individually cloned into the MCSs of the empty pTT5Multi vector, generating two plasmids, pTT5Multi-Gene1 and pTT5Multi-Gene2. Then, pTT5Multi-Gene1 was double digested with AvrII and MluI, while pTT5Multi-Gene2 was double digested with SpeI and MluI. After double digestion, as AvrII and SpeI were isocaudomers, the backbone containing Gene1 cassette was ligated with the fragment containing Gene2 cassette to give rise to the plasmid pTT5Multi-Gene1-Gene2. Since the plasmid pTT5Multi-Gene1-Gene2 still contains the SpeI, AvrII, and MluI sites, this process can be repeated to add more gene cassettes. (C) Schematic diagram of two pTT5Multi plasmids that contain indicated components of human augmin and three pTT5Multi plasmids that contain indicated components of human γ -TuRC. H, HAUS. Tags for augmin in this study: GFP-Strep, mCherry-Strep, SNAP-Strep, and GFP-Bio. Tags for γ -TuRC in this study: GFP and GFP-Strep. NEDD1 was highlighted with a dashed box because it was removed for experiments with γ -TuRC ^{Δ NEDD1}. (D) Coomassie blue-stained gel with recombinant augmin-GFP complex purified from nocodazole-arrested mitotic HEK293T cells coexpressing pTT5Multi-H6-GFP-Strep/H2/H8/H3 and pTT5Multi-H7/H5/H4/H1. (E) Coomassie blue-stained gel with recombinant γ -TuRC-GFP complex purified from nocodazole-arrested mitotic HEK293T cells coexpressing pTT5Multi-GCP3-GFP-Strep/GCP2/ γ -tubulin/ γ -tubulin, pTT5Multi-GCP4/GCP6/GCP5, and pTT5Multi-MZT2A/MZT2B/MZT1/NME7/NEDD1. (F) TIRF microscopy images of de novo nucleation of MTs (red) from solution in the presence of recombinant γ -TuRC-GFP complex (green) at indicated concentrations. Images were acquired 10 min after imaging. (G) Quantification of the total MT number per 1,000 μ m² for experiments shown in F. $n = 3$ experiments. (H) Plots of the total MT number per 1,000 μ m² at indicated time points for experiments shown in F. $n = 3$ experiments. (I and J) Quantification of intensities of augmin-mCherry (I) and γ -TuRC-GFP (J) along MTs for the experiments shown in Fig. 3 G. The values were normalized to the intensity of augmin-mCherry alone (I) or γ -TuRC-GFP alone (J). $n = 60$ MTs from three experiments. (K) Coomassie blue-stained gel with recombinant complete augmin- γ -TuRC complex copurified from nocodazole-arrested mitotic HEK293T cells coexpressing augmin-mCherry-Strep and γ -TuRC-GFP. (L) TIRF microscopy images showing robust branching MT nucleation in the presence of recombinant complete augmin-mCherry-Strep- γ -TuRC-GFP complex (10 nM augmin; 0.62 nM γ -TuRC). (M) Quantification of the total number of branched MTs per fan-like structure at indicated time points for the experiments shown in L. $n = 3$ experiments. (N) Distribution of branch angles for the experiments shown in L. $n = 300$ branch angles from four experiments. (O) Coomassie blue-stained gels with recombinant complete augmin- γ -TuRC complexes copurified from nocodazole-arrested mitotic HEK293T cells expressing augmin-mCherry-Strep and γ -TuRC-GFP, together with or without untagged CDK1/cyclin B, HA-PLK1, or both. Scale bars, 2 μ m. Data represent mean \pm SD.

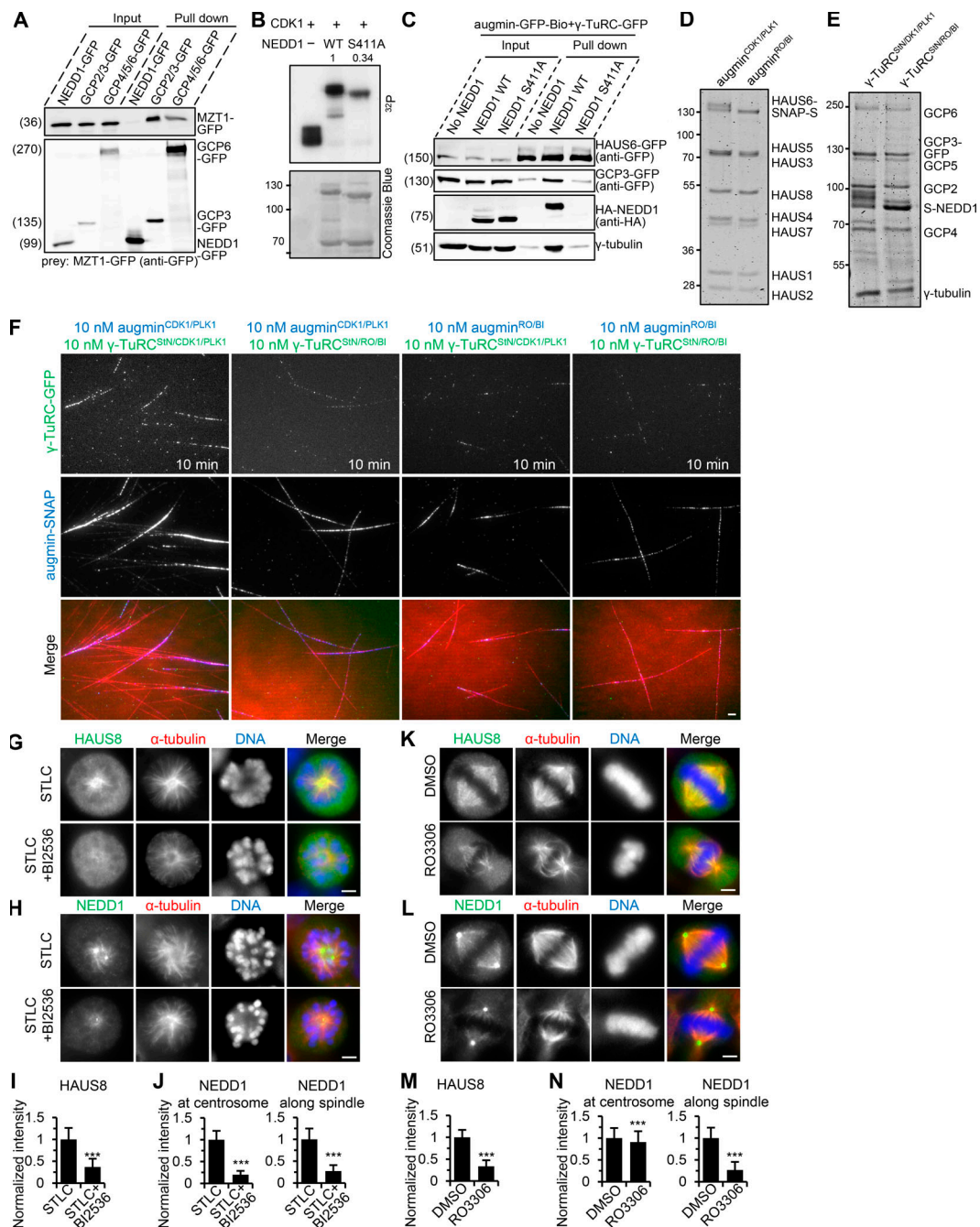


Figure S4. PLK1- and CDK1-dependent phosphorylation is essential for branching MT nucleation in vitro and important for the spindle localization of augmin and γ -TuRC in cells. (A) Streptavidin pull-down assay with extracts of nocodazole-arrested mitotic HEK293T cells expressing MZT1-GFP (prey) together with NEDD1-GFP-Bio, GCP2/GCP3-GFP-Bio/ γ -tubulin, or GCP4/GCP5/GCP6-GFP-Bio/ γ -tubulin (bait), analyzed by Western blotting with GFP antibody. (B) Purified GFP-NEDD1, both WT and S411A mutant, were phosphorylated in vitro using [32 P]ATP and active CDK1/cyclin B (see Materials and methods for details). Kinase assay reaction products were separated by SDS-PAGE (lower panel) and visualized by autoradiography (upper panel). The CDK1/cyclin B kinase alone was used as the positive control. The S411A mutation reduced the level of NEDD1 phosphorylation by 66%. (C) Streptavidin pull-down assay with extracts of nocodazole-arrested mitotic HEK293T cells expressing augmin-GFP-Bio (bait) together with γ -TuRC^{NEDD1}-GFP, WT, or S411A mutant of γ -TuRC-GFP (prey), analyzed by Western blotting with indicated antibodies. (D and E) Coomassie blue-stained gels with augmin-SNAP (D) and γ -TuRC^{SIN/RO/BI}-GFP (E) that were purified from nocodazole-arrested mitotic HEK293T cells in the presence of either coexpressed untagged CDK1/cyclin B and HA-PLK1, or the combined inhibitors (augmin^{CDK1/PLK1}, augmin^{RO/BI}, γ -TuRC^{SIN/CDK1/PLK1}, and γ -TuRC^{SIN/RO/BI}). (F) TIRF microscopy images showing robust branching MT nucleation in the presence of the pair of 10 nM augmin^{CDK1/PLK1}-SNAP (blue) and 10 nM γ -TuRC^{SIN/CDK1/PLK1}-GFP (green), but not other pairs. Scale bar, 2 μ m. (G–J) Immunofluorescence staining and quantification of HAUS8 intensity along the spindle (G) as well as NEDD1 intensity at the centrosome or along the spindle (H) in HeLa cells treated with or without BI2536 (300 nM) for 2 h and with STLC for 4 h. The values were normalized to the intensity of HeLa cells treated only with STLC. $n = 50$ cells. (K–N) Immunofluorescence staining and quantification of HAUS8 intensity along the spindle (K) as well as NEDD1 intensity at the centrosome or along the spindle (L) in HeLa cells treated with DMSO (control) or RO3306 (10 μ M) for 30 min. The values were normalized to the intensity of DMSO-treated HeLa cells. $n = 50$ cells. Scale bars, 2 μ m. Data represent mean \pm SD. ***, $P < 0.001$, two-tailed t test.

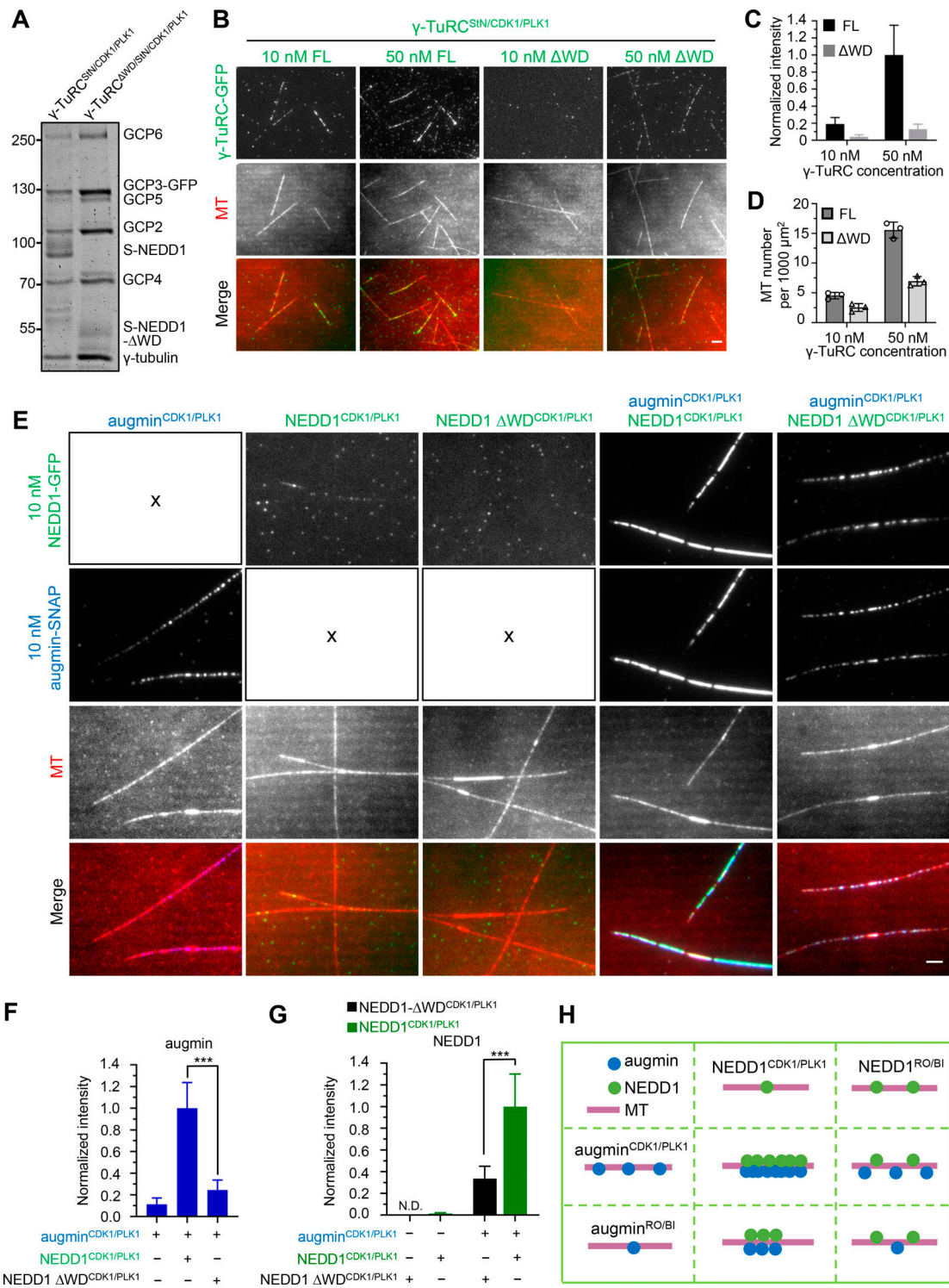


Figure S5. Characterization of the contribution of NEDD1 WD to γ -TuRC's nucleation activity and the synergistic MT-binding activities between NEDD1 and augmin. (A) Coomassie blue-stained gel with purified γ -TuRC^{S_N/CDK1/PLK1}-GFP and γ -TuRC^{ΔWD/S_N/CDK1/PLK1}-GFP. (B) TIRF microscopy images of de novo nucleation of MTs from solution in the presence of γ -TuRC^{S_N/CDK1/PLK1}-GFP (FL) or γ -TuRC^{ΔWD/S_N/CDK1/PLK1}-GFP (ΔWD) at indicated concentrations. (C) Quantification of intensities of γ -TuRC^{S_N/CDK1/PLK1}-GFP (FL) and γ -TuRC^{ΔWD/S_N/CDK1/PLK1}-GFP (ΔWD) along MTs for experiments shown in B. The values were normalized to the intensity of 50 nM γ -TuRC^{S_N/CDK1/PLK1}-GFP. *n* = 60 MTs from three experiments. (D) Quantification of the total MT number per 1,000 μ m² for experiments shown in B. *n* = 3 experiments. (E) TIRF microscopy images of MTs (red) grown in the presence of 10 nM augmin^{CDK1/PLK1}-SNAP (blue), 10 nM NEDD1^{CDK1/PLK1}-GFP (green), 10 nM NEDD1 Δ WD^{CDK1/PLK1}-GFP (green), either alone or combined in pairs. (F and G) Quantification of intensities of augmin^{CDK1/PLK1}-SNAP (F) as well as NEDD1^{CDK1/PLK1}-GFP and NEDD1 Δ WD^{CDK1/PLK1}-GFP (G) along MTs for experiments shown in E. The values were normalized to the intensities of the augmin^{CDK1/PLK1}-SNAP and NEDD1^{CDK1/PLK1}-GFP pair. N.D., not detected. *n* = 50 MTs from three experiments. (H) Schematic diagram showing the MT-binding activity of different versions of augmin (augmin^{CDK1/PLK1} and augmin^{RO/BI}) and NEDD1 (NEDD1^{CDK1/PLK1} and NEDD1^{RO/BI}), either alone or combined in pairs. Scale bars, 2 μ m. Data represent mean \pm SD. ***, *P* < 0.001, two-tailed *t* test.

Video 1. **Reconstitution of branching MT nucleation using purified native augmin- γ -TuRC complex.** Branching MT nucleation both from GMPCPP seeds (tracked by arrows) and from solution (tracked by arrowhead) in the presence of native augmin- γ -TuRC complex (10 nM augmin; 0.35 nM γ -TuRC) purified from nocodazole-arrested mitotic HAUS8-GFP-Strep knock-in HeLa cells. Images were collected with a TIRF microscope at 4-s intervals. Video is sped up 160 times (40 frames/s). Time is shown in the format min:s. Scale bars, 5 μ m.

Video 2. **A closer inspection of branching events occurred from a single GMPCPP seed.** Primary, secondary, and tertiary branching events occurred in an ordered series in the presence of native augmin- γ -TuRC complex (10 nM augmin; 0.35 nM γ -TuRC) purified from nocodazole-arrested mitotic HAUS8-GFP-Strep knock-in HeLa cells. Images were collected with a TIRF microscope at 4-s intervals. Video is sped up 160 times (40 frames/s). Time is shown in the format min:s. Scale bars, 5 μ m.

Video 3. **Direct observation of augmin and γ -TuRC during the process of branching nucleation.** Branching MT nucleation in the presence of native augmin- γ -TuRC complex (7.5 nM augmin; 0.15 nM γ -TuRC) purified from nocodazole-arrested mitotic HAUS8-GFP-Strep/GCP2-SNAP double knock-in HeLa cells. Images were collected with a TIRF microscope at 4-s intervals. Video is sped up 160 times (40 frames/s). Time is shown in the format min:s. Scale bars, 5 μ m.

Video 4. **A closer inspection of augmin and γ -TuRC during the process of branching nucleation.** Branching MT nucleation in the presence of native augmin- γ -TuRC complex (7.5 nM augmin; 0.15 nM γ -TuRC) purified from nocodazole-arrested mitotic HAUS8-GFP-Strep/GCP2-SNAP double knock-in HeLa cells. Images were collected with a TIRF microscope at 4-s intervals. Video is sped up 160 times (40 frames/s). Time is shown in the format min:s. Scale bars, 5 μ m.

Video 5. **MT nucleation at different γ -TuRC concentrations.** MT nucleation in the presence of indicated concentrations of γ -TuRC-GFP (green). Each arrow indicates an MT minus end capped by a γ -TuRC-GFP spot. Images were collected with a TIRF microscope at 2-s intervals. Video is sped up 80 times (40 frames/s). Time is shown in the format min:s. Scale bars, 5 μ m.

Video 6. **Reconstitution of branching MT nucleation using recombinant complete augmin- γ -TuRC complex.** Branching MT nucleation in the presence of recombinant complete augmin- γ -TuRC complex (10 nM augmin; 0.62 nM γ -TuRC) copurified from nocodazole-arrested mitotic HEK293T cells coexpressing augmin-mCherry-Strep and γ -TuRC-GFP. Images were collected with a TIRF microscope at 4-s intervals. Video is sped up 160 times (40 frames/s). Time is shown in the format min:s. Scale bars, 5 μ m.

Video 7. **A closer inspection of branching MT nucleation using recombinant complete augmin- γ -TuRC complex.** Shows a smaller field of view corresponding to [Video 6](#).

Video 8. **Reconstitution of more robust branching MT nucleation using recombinant complete augmin- γ -TuRC complex phosphorylated by CDK1 and PLK1.** Branching MT nucleation in the presence of recombinant complete augmin- γ -TuRC complex (10 nM augmin; 1.0 nM γ -TuRC) copurified from nocodazole-arrested mitotic HEK293T cells expressing augmin-mCherry-Strep and γ -TuRC-GFP, together with untagged CDK1/cyclin B and HA-PLK1. Images were collected with a TIRF microscope at 4-s intervals. Video is sped up 160 times (40 frames/s). Time is shown in the format min:s. Scale bars, 5 μ m.

Video 9. **Both augmin phosphorylation and γ -TuRC phosphorylation by CDK1 and PLK1 are required for robust branching MT nucleation.** Branching MT nucleation in the presence of four pairs of 10 nM augmin-SNAP (blue) and 10 nM γ -TuRC-GFP^{StN} (green), either in phosphorylated or nonphosphorylated form. Augmin-SNAP and γ -TuRC-GFP^{StN} were separately purified from nocodazole-arrested mitotic HEK293T cells in the presence of either coexpressed untagged CDK1/cyclin B and HA-PLK1 or the combined inhibitors (augmin^{CDK1/PLK1}, augmin^{RO/BI}, γ -TuRC^{StN/CDK1/PLK1}, and γ -TuRC^{StN/RO/BI}). Images were collected with a TIRF microscope at 4-s intervals. Video is sped up 160 times (40 frames/s). Time is shown in the format min:s. Scale bars, 5 μ m.

Video 10. **NEDD1 WD40 domain is essential for branching nucleation.** Branching MT nucleation in the presence of 10 nM augmin-SNAP (blue) together with 10 nM γ -TuRC-GFP^{StN} or indicated concentrations of γ -TuRC ^{Δ WD/StN}-GFP (green), all in phosphorylated forms. These complexes were separately purified from nocodazole-arrested mitotic HEK293T cells in the presence of coexpressed untagged CDK1/cyclin B and HA-PLK1 (augmin^{CDK1/PLK1}, γ -TuRC^{StN/CDK1/PLK1}, and γ -TuRC ^{Δ WD/StN/CDK1/PLK1}). Images were collected with a TIRF microscope at 4-s intervals. Video is sped up 160 times (40 frames/s). Time is shown in the format min:s. Scale bars, 5 μ m.

Provided online are Table S1 and Table S2. Table S1 shows the analysis of native augmin- γ -TuRC complex, recombinant augmin complex, recombinant γ -TuRC, and recombinant augmin- γ -TuRC complex used for in vitro assay by mass spectrometry. Table S2 provides a brief overview of the tagging and purification strategies used in this study.